2016

Probing the electroweak phase transition at the LHC

Peisi Huang
University of Chicago, peisi.huang@unl.edu

Aniket Joglekar
University of Chicago

Bing Li
University of Chicago

Carlos E. M. Wagner
University of Chicago, cwagner@hep.anl.gov

PHYSICAL REVIEW D **93,** 055049 (2016)

Probing the electroweak phase transition at the LHC

Peisi Huang,[1,3] Aniket Joglekar,[1] Bing Li,[1] and Carlos E. M. Wagner[1,2,3]
[1]*Enrico Fermi Institute, University of Chicago, Chicago, Illinois 60637, USA*
[2]*Kavli Institute for Cosmological Physics, University of Chicago, Chicago, Illinois 60637, USA*
[3]*HEP Division, Argonne National Laboratory, 9700 Cass Avenue, Argonne, Illinois 60439, USA*
(Received 22 December 2015; published 31 March 2016)

We study the correlation between the value of the triple Higgs coupling and the nature of the electroweak phase transition. We use an effective potential approach, including higher order, nonrenormalizable terms coming from integrating out new physics. We show that if only the dimension six operators are considered, large positive deviations of the triple Higgs coupling from its standard model (SM) value are predicted in the regions of parameter space consistent with a strong first order electroweak phase transition. We also show that at higher orders sizable and negative deviations of the triple Higgs coupling may be obtained, and the sign of the corrections tends to be correlated with the order of the phase transition. We also consider a singlet extension of the SM, which allows us to establish the connection with the effective field theory approach and analyze the limits of its validity. Furthermore, we study how to probe the triple Higgs coupling from the double Higgs production at the LHC. We show that selective cuts in the invariant mass of the two Higgs bosons should be used, to maximize the sensitivity for values of the triple Higgs coupling significantly different from the standard model one.

DOI: 10.1103/PhysRevD.93.055049

I. INTRODUCTION

After the Higgs discovery at the LHC [1,2], the Higgs properties, including the Higgs mass and the Higgs couplings to the standard model (SM) particles, were measured [3–5]. Those measurements show that the Higgs boson properties are close to the SM ones. Those properties are related to the gauge transformation properties of the Higgs field and with the mechanism of electroweak symmetry breaking, but provide little information about the properties of the Higgs potential. In the SM, a quadratic coupling and a quartic coupling completely specify this potential. In the theories beyond the SM, there can be contributions to the effective potential from the higher dimensional operators, with an effective cutoff given by the characteristic new physics scale of the theory. As a result, the self interactions of the Higgs field, most notably the triple Higgs coupling (λ_3), are modified.

What makes the deviation of λ_3 from its SM value even more exciting is that λ_3 is closely related to the strength of the electroweak phase transition (EPT) [6–13]. Understanding the nature of the EPT will advance our knowledge of the possible realization of electroweak baryogenesis [14], which is an attractive explanation of the baryon antibaryon asymmetry, that can only happen if the EPT is first order. Today the electroweak symmetry is clearly broken, while in the early Universe the $SU(2) \times U(1)$ symmetry was preserved, a result that may be easily understood considering the finite temperature effects to the effective potential. About 10^{-10} seconds after the big bang, the Universe underwent a phase transition from the unbroken phase to the broken phase. This leads to formation and expansion of bubbles of the true vacuum configuration in the false, gauge symmetric vacuum. In the presence of charge parity violation, particle interactions with the expanding bubbles may lead to the creation of an excess of baryons inside the bubbles by means of baryon number violating processes induced by sphalerons [15]. These sphaleron processes, if they were in equilibrium inside the bubbles, would wipe off the created excess of baryons. The rate of these processes depends exponentially on the ratio of the vacuum expectation value (VEV) to the critical temperature at the time of the phase transition and is suppressed if the phase transition is of strong first order [16]. Unfortunately, in the pure SM scenario, the requirement of a sufficiently strong first order phase transition translates into an upper bound on the Higgs mass of about 35 GeV [17,18]. The discovery of the Higgs boson at 125 GeV excludes such a simple scenario [1,2]. This motivates a further investigation of the viability of the electroweak baryogenesis in minimally extended scenarios.

A first order electroweak phase transition (FOEPT) may lead to the production of gravitational waves, but the characteristic scales associated with it make their detection very difficult, albeit not impossible, to detect in the near future [19–25]. Alternatively, the models that lead to a FOEPT through a relevant modification of the zero temperature effective potential can be probed from the deviation of λ_3 from its SM value, as suggested in previous studies [8,11,12].

At the LHC, λ_3 can be probed by the process of double Higgs production. Mainly due to the destructive interference between the one-loop diagrams, the production cross section reduces initially, as the λ_3 is enhanced from its SM

value. At the next-to-leading order (NLO), the minimum occurs for $\lambda_3 \sim 2.45\lambda_3^{\rm SM}$ [26]. Further enhancement of the λ_3 value increases the cross section again, which exceeds the SM value for $\lambda_3 > 5\lambda_3^{\rm SM}$. The cross section also increases if the correction to $\lambda_3^{\rm SM}$ is negative. The $b\bar{b}\gamma\gamma$, $b\bar{b}\tau^+\tau^-$, $b\bar{b}W^+W^-$ and $bb\bar{b}\,\bar{b}$ channels [27–35] have been studied. These studies showed that around 50% accuracy can be achieved from the $b\bar{b}\gamma\gamma$ channel alone assuming that λ_3 is not too far away from its SM value and the acceptance for different values of λ_3 stays the same. However, as pointed out in [31], the acceptance drops significantly for large values of λ_3. In this article we perform a detailed study of the impact of a large deviation from $\lambda_3^{\rm SM}$ on the double Higgs production process. We also present an analysis of the LHC searches for this process including relevant QCD background contributions that have been overlooked in the previous studies.

The organization of this article is as follows: In Sec. II, we calculate the values of λ_3 if the EPT is first order in a simplified model, where we include higher order terms in the effective potential. In Sec. III, we compare our results to those obtained in singlet extensions like the ones that may be obtained from the scalar Higgs sector in the next to minimal supersymmetric standard model (NMSSM). In Sec. IV, we discuss the measurement of λ_3 at the LHC, for the SM-like values as well as for values of λ_3 that present a large positive or negative deviation with respect to the SM value. We reserve Sec. V for the conclusions and some technical details for the appendixes.

II. THE EFFECTIVE POTENTIAL AND THE TRILINEAR HIGGS COUPLING

A modification of the nature of the phase transition may be achieved by adding extra terms to the Higgs potential [36–38]. These may appear through relevant temperature dependent modifications of the Higgs potential, beyond those associated with the increase of the effective mass parameter, which lead to the symmetry restoration phenomenon (see, for example, Refs. [39–54]).

Alternatively, these effects may be already present at zero temperature, through additional terms in the Higgs potential induced by integrating out new physics at the scales above the weak scale. In this section we concentrate on the second possibility and illustrate the impact of such additional terms on the enhancement of λ_3 in minimally extended models. Several simple extensions of the SM are capable of generating the required extra terms in the potential and have been studied in the literature [6–13, 55–59]. In Sec. III, we analyze one such example, where a gauge singlet is added to the SM. This can lead to a relevant modification of the trilinear Higgs coupling with respect to the SM value $\lambda_3^{\rm SM}$, even for values of the singlet mass much larger than the weak scale. In such a case, the singlet decouples from physics processes at the LHC, allowing a comparison of these results with the ones obtained in the effective low energy field theory.

In this section, we take a general approach to the effective field theory (EFT), where nonrenormalizable terms are added to the Higgs potential. We investigate whether these can potentially generate considerably larger cross sections for the $gg \to hh$ process compared to the standard model. We also explore the possibility of these being compatible with a strongly first order electroweak phase transition (SFOEPT). Such modifications to $\lambda_3^{\rm SM}$ would make for a viable probe to the new physics at the LHC and beyond.

A. Nonrenormalizable terms in the low energy Higgs potential

The general formalism in this section is as follows. All the tree-level effective operators represented by powers of $(\phi^\dagger\phi)$ are added to the usual Higgs potential at the temperature $T = 0$ as follows,

$$V(\phi, 0) = \frac{m^2}{2}(\phi^\dagger\phi) + \frac{\lambda}{4}(\phi^\dagger\phi)^2 + \sum_{n=1}^{\infty} \frac{c_{2n+4}}{2^{(n+2)}\Lambda^{2n}}(\phi^\dagger\phi)^{n+2}, \quad (1)$$

where $\phi = v + h$ and hence the VEV is given as $\langle\phi\rangle = 246$ GeV. This leads to a correction to the SM value of the triple Higgs coupling as shown in Appendix A,

$$\lambda_3 = \frac{3m_h^2}{v}\left(1 + \frac{8v^2}{3m_h^2}\sum_{n=1}^{\infty}\frac{n(n+1)(n+2)c_{2n+4}v^{2n}}{2^{n+2}\Lambda^{2n}}\right). \quad (2)$$

The nonzero temperature effects are approximately accounted for by adding a thermal mass correction term to the Higgs potential. This term is generated in the high-T expansion of the one-loop thermal potential. At temperature T, we get $m^2(T) = m^2 + a_0T^2$. We have ignored the small cubic term contributions as well as the logarithmic contributions as they are suppressed compared to the contributions from higher order terms. Here we have assumed that the heavy new physics is not present in the EFT at the weak scale and therefore its contribution is Boltzmann suppressed at the EPT scale. In such a case a_0 is a constant proportional to the square of SM gauge and Yukawa coupling constants. Assuming all $c_{2n} \simeq 1$, the minimum value that Λ can achieve is 174 GeV in this formulation, at which point the convergence of the series is lost for values of ϕ close to its VEV. However, in any consistent EFT, the cutoff scale Λ is considerably higher than 174 GeV.

Using Eq. (2), we define another quantity δ which quantifies the deviations of the trilinear Higgs coupling with respect to the SM value as

$$\delta = \frac{\lambda_3}{\lambda_3^{\rm SM}} - 1 = \frac{8v^2}{3m_h^2}\sum_{n=1}^{\infty}\frac{n(n+1)(n+2)c_{2n+4}v^{2n}}{2^{n+2}\Lambda^{2n}}, \qquad (3)$$

where we restrict $|c_{2n+4}| < 1$.

The values of the enhancement of λ_3 for a given Λ for all potentials satisfying these conditions are shown in Fig. 1. This maximal possible value, shown in the uppermost black (dashed) line in all the panels in Fig. 1, is obtained assuming all $c_{2n} = 1$ and leads to a large enhancement even at a relatively large value of Λ. However, the only condition that we have imposed on the potential so far is the existence of a local minimum with a second derivative consistent with the measured Higgs mass $m_h \simeq 125$ GeV. For this minimum to represent the physical vacuum of the theory, however, it should be a global one. As we show, the global minimum requirement imposes strong constraints on the possible enhancement of the triple Higgs coupling.

In our further analysis, we choose not to consider the terms of the order higher than $(\phi^\dagger\phi)^5$ as they introduce negligible corrections for the cutoffs higher than v as shown in Fig. 1. We separately analyze the nature of the phase transition and the maximum positive and negative values for δ in each of the three cases corresponding to $(\phi^\dagger\phi)^3$, $(\phi^\dagger\phi)^4$ and $(\phi^\dagger\phi)^5$. Let us stress that these momentum independent operators preserve the custodial symmetry and evade the tight phenomenological constraints coming from the ρ parameter. The momentum dependent non-renormalizable operators [13,60–62], instead, may contribute to the oblique corrections and are very tightly

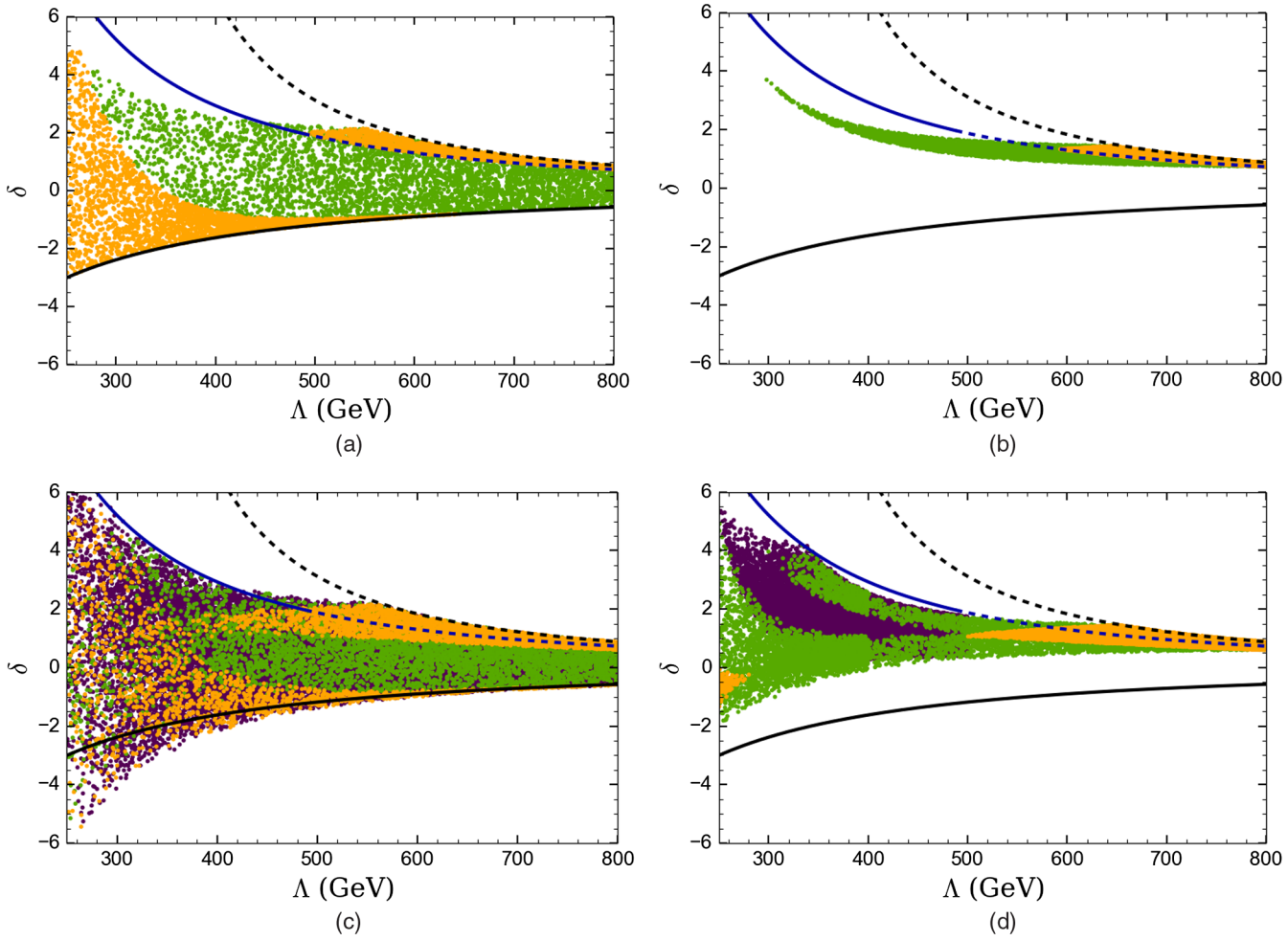

FIG. 1. Triple Higgs coupling correction δ as a function of the cutoff Λ. The upper dashed black line shows the maximum value of δ for the infinite sum with all $|c_{2n}| = 1$. The dashed dark blue shows the values consistent with a FOEPT for the $(\phi^\dagger\phi)^3$ potential extension, for $c_6 = 1$, while for the same conditions the solid light blue line is forbidden due to the absence of electroweak symmetry breakdown. Figures 1(a)–1(b) show the results for the $(\phi^\dagger\phi)^4$ potential. The different colors correspond to the different hierarchies of the effective potential coefficients as explained in the text. Figure 1(a) shows the general case while Fig. 1(b) shows the result if a FOEPT is demanded. Figures 1(c)–1(d) show similar results but for the $(\phi^\dagger\phi)^5$ potential, with different colors again corresponding to different coefficient hierarchies defined in the text. The lower solid black line shows the maximal negative values of δ possible for the order $(\phi^\dagger\phi)^4$ potential.

constrained by the electroweak precision measurements. A particularly relevant one for our analysis is

$$\frac{c_H}{8\Lambda^2}\partial_\mu(\phi^\dagger\phi)\partial^\mu(\phi^\dagger\phi). \tag{4}$$

This correction plays a relevant role in the singlet case that we discuss below, but is also restricted by the measurement of the Higgs production rate and tends to be small, which will be discussed later. Hence, in most of our analysis we ignore the momentum dependent corrections but we consider them in the comparison with the singlet case in Sec. III B.

1. Higgs potential of order $(\phi^\dagger\phi)^3$

From Eqs. (1)–(2), the potential and the triple Higgs coupling are given by

$$V(\phi,T)=\frac{m^2+a_0T^2}{2}(\phi^\dagger\phi)+\frac{\lambda}{4}(\phi^\dagger\phi)^2+\frac{c_6}{8\Lambda^2}(\phi^\dagger\phi)^3, \tag{5}$$

$$\lambda_3=\frac{3m_h^2}{v}\left(1+\frac{2c_6v^4}{m_h^2\Lambda^2}\right). \tag{6}$$

This case has been studied in the literature in various contexts [6–13,63,64]. We point out a few key things pertaining to this case in the present context.

We require $c_6>0$ for the stability of the potential.[1] The requirement that there should be a minimum of the potential at $\phi=\phi_c$ degenerate with the extreme at $\phi=0$ for the temperature $T=T_c$ leads to

$$\lambda^2=4m^2(T_c)\frac{c_6}{\Lambda^2}. \tag{7}$$

This implies that $m^2(T)$, which is the curvature of the potential at $\phi=0$, should be greater than zero at $T=T_c$ for the phase transition to be of the first order. The minimum of the potential at the critical temperature is at

$$(\phi_c^\dagger\phi_c)=v_c^2=-\frac{\lambda\Lambda^2}{c_6}. \tag{8}$$

This implies that an additional condition to obtain a FOEPT is that the effective quartic coupling should be negative, namely $\lambda<0$.

The value of the Higgs mass imposes a relation between λ and c_6, namely

$$\lambda+\frac{3c_6}{2\Lambda^2}v^2=\frac{m_h^2}{2v^2}. \tag{9}$$

Using Eqs. (8)–(9) gives

$$\frac{c_6}{\Lambda^2}=\frac{m_h^2}{3v^2(v^2-\frac{2}{3}v_c^2)}, \tag{10}$$

from where all coefficients m^2, λ and c_6 may be written in terms of the m_h, v_c and v. Using these relations one obtains

$$T_c^2=\frac{3c_6}{4\Lambda^2a_0}(v^2-v_c^2)\left(v^2-\frac{v_c^2}{3}\right). \tag{11}$$

Demanding both c_6 and T_c^2 to be positive, we get $v_c<v$. This translates into an upper bound on c_6 using Eq. (10),

$$\frac{c_6}{\Lambda^2}<\frac{m_h^2}{v^4}. \tag{12}$$

Then from Eq. (6), we conclude that the coupling can be enhanced by a factor of 3 at most. Moreover, demanding $v_c^2>0$, or equivalently $\lambda<0$, puts an additional constraint on the obtention of a FOEPT, namely

$$\frac{c_6}{\Lambda^2}>\frac{m_h^2}{3v^4} \tag{13}$$

which implies a minimal enhancement of a factor two thirds.

This implies that a FOEPT may only be obtained if the following conditions are fulfilled:

$$\frac{2}{3}\le\delta\le 2. \tag{14}$$

Moreover, for $c_6=1$, Eqs. (12)–(13) imply a bound on the effective cutoff Λ, namely

$$\frac{v^2}{m_h}<\Lambda<\frac{\sqrt{3}v^2}{m_h}, \tag{15}$$

which correspond to upper and lower bounds on Λ of approximately 484 and 838 GeV respectively, and larger enhancement δ is obtained for the smaller values of the cutoff. The phase transition becomes stronger first order for smaller values of the cutoff and becomes a weakly first order one for values of Λ close to the upper bound in Eq. (15). Let us stress that for values of Λ below the lower bound in Eq. (15), $\Lambda<484$ GeV, the minimum at $T=0$ is no longer a global minimum and hence electroweak symmetry breaking does not occur.

In Fig. 1, we show the possible triple Higgs coupling enhancement factor δ as a function of the cutoff Λ for different extensions of the SM effective potential. The

[1]We understand that even for $c_6<0$ the stability could be recovered for field values that are above the cutoff, where the EFT is not valid. We consider the case of $c_6<0$ when we study the $(\phi^\dagger\phi)^{4,5}$ extensions.

particular case of the potential of order $(\phi^\dagger\phi)^3$ is represented by the blue curve. The maximum enhancement $\lambda_3 = 3\lambda_3^{\rm SM}$ is achieved at $\Lambda \sim 484$ GeV. For the cutoffs above $\Lambda \sim 838$ GeV, not shown in the figure, the phase transition is not first order anymore, but the Higgs potential is still a viable one. Note that the low value of the cutoff does not necessarily correspond to any physical mass scale, as is discussed in the singlet case, in Sec. III.

Let us note before closing that in Ref. [65] it is found that for a FOEPT to take place, the enhancement due to a six-dimensional operator to the Higgs potential cannot be larger than ∼20%. In order to understand the difference between their result and ours we notice that in their normalization, the coefficient of the $(\phi^\dagger\phi)^3$ term is written as $\frac{\bar{c}_6\lambda}{f^2}$, where λ is the coefficient of the $(\phi^\dagger\phi)^2$ term.[2] The discrepancy is due to the assumption in Ref. [65] that $\bar{c}_6 > 0$ and $\bar{c}_6 v^2/f^2$ is small. As we showed above, for a FOEPT to take place, the effective quartic coupling $\lambda < 0$, which means $\bar{c}_6 < 0$ is required for the stability of the potential. Also, for $\lambda < 0$, the required condition to obtain a positive Higgs mass is $\bar{c}_6 v^2/f^2 < -\frac{2}{3}$. Thus, in the notation of Ref. [65], $|\bar{c}_6| v^2/f^2$ cannot be used as a small expansion parameter in the region of parameters consistent with a FOEPT. Finally, the upper bound assumed on $\bar{c}_6/\Lambda^2$, coming from Ref. [7], is similar to the one we derived in Eq. (12) and is applicable to c_6/Λ^2 and not to $\bar{c}_6/\Lambda^2$.

2. Higgs potential of order $(\phi^\dagger\phi)^4$

From Eqs. (1)–(2), the potential and the triple Higgs coupling are

$$V(\phi,T) = \frac{m^2 + a_0 T^2}{2}(\phi^\dagger\phi) + \frac{\lambda}{4}(\phi^\dagger\phi)^2 + \frac{c_6}{8\Lambda^2}(\phi^\dagger\phi)^3 + \frac{c_8}{16\Lambda^2}(\phi^\dagger\phi)^4, \tag{16}$$

$$\lambda_3 = \frac{3m_h^2}{v}\left(1 + \frac{2c_6 v^4}{m_h^2\Lambda^2} + \frac{4c_8 v^6}{m_h^2\Lambda^4}\right). \tag{17}$$

This case is particularly interesting because contrary to the $(\phi^\dagger\phi)^3$ case, the trilinear Higgs couplings may be either enhanced or suppressed and one can even get an inversion of the sign of λ_3 with respect to $\lambda_3^{\rm SM}$. As mentioned before, a suppression or change of sign of λ_3 would be interesting from the collider perspective as it avoids the problem of a strong destructive interference between the box and the triangle diagrams for $gg \to hh$.

The orange and green regions in Figs. 1(a)–1(b) correspond to the regions consistent with the experimental values of the Higgs mass and the Higgs VEV. Figure 1(a) shows the possible modifications (δ) of the $\lambda_3^{\rm SM}$ possible in this case. Figure 1(b) outlines the region in Fig. 1(a) which corresponds to the FOEPT. This shows that an inversion of sign or suppression of λ_3 with respect to $\lambda_3^{\rm SM}$ necessarily implies that the phase transition is not a first order one. In the construction of Fig. 1(b), we have not considered the region of the parameter space corresponding to potentials with barriers between the minima at $\phi = 0$ and $\phi = v$ at $T = 0$. This is due to the fact that a metastability analysis would be required to determine the part of this region in which a FOEPT takes place. Therefore, this rather small region is neglected in our analysis. As a result of this, a small part of the dashed blue curve is not surrounded by the shaded regions. The same is true for Fig. 1(d).

In Figs. 1(a)–1(b), the different colors indicate different regions of the parameter space. The orange region corresponds to $|c_6| = 1$, $0 < c_8 < 1$, while the green region corresponds to $|c_6| < 1$, $c_8 = 1$. The regions can overlap, because a different combination of c_6 and c_8 can produce the same value of δ for the same cutoff. In fact, beneath all of the orange region above the blue curve there exists a green region. We observe that it is possible to obtain λ_3 values ranging from $-2\lambda_3^{\rm SM}$ to $6\lambda_3^{\rm SM}$ for cutoffs higher than 250 GeV. Demanding a FOEPT reduces it to a smaller range from $\frac{5}{3}\lambda_3^{\rm SM}$ to $5\lambda_3^{\rm SM}$. We also note from Fig. 1(b) that the FOEPT has a lower bound on the cutoff ∼300 GeV, which is somewhat lower than in the $(\phi^\dagger\phi)^3$ case. Note that the contribution to λ_3 from the dimension-8 operators is suppressed compared to that from the dimension-6 operators. The fact that in a $(\phi^\dagger\phi)^4$ theory, λ_3 has a much larger range in the general case compared to a $(\phi^\dagger\phi)^3$ theory, and in the region consistent with the FOEPT is because with c_8 being a positive number, c_6 is allowed to take negative values in the range of $|c_6| < 1$ in a $(\phi^\dagger\phi)^4$ theory, while $0 < c_6 < 1$ has to be fulfilled in a $(\phi^\dagger\phi)^3$ theory.

Let us stress that negative values of δ imply that the curvature is decreasing at $\phi = v$. If this behavior is preserved at larger values of ϕ, one would expect a maximum of the potential for $\phi > v$. Then the stability of the potential means there has to be one more minimum for $\phi > v$. The deeper the extra minimum, the more negative the value of λ_3. Thus, demanding the physical minimum to be a global one, a maximal negative value would occur at the point where both minima have the same potential value. In order to retain the analytic control, we plot the analytical bound coming from the point marking the end of the absolute stability. For the $(\phi^\dagger\phi)^4$ case, this bound is the black curve at the bottom of each panel of Fig. 1. As shown in Appendix B, this maximally negative enhancement is given as

$$\delta > -\frac{x}{1+\sqrt{1+x}}, \quad \text{where } x = \frac{4v^4}{m_h^2\Lambda^2}. \tag{18}$$

[2]We denote the coefficient used in Ref. [65] $\bar{c}_6$, not to confuse it with the coefficient c_6 defined above.

Observe, however, that for $\Lambda \simeq 250$ GeV the second minimum would occur at values of ϕ of order or larger than Λ, and hence this analytical result should be taken with care. The numerical results of Fig. 1 were obtained by only demanding the physical minimum to be the global one. The largest negative enhancements obtained numerically are consistent with the predictions of Eq. (18) up to values of $\Lambda \simeq v$. Let us stress again that although we show examples with very low cutoff values, those low cutoff values may be hard to realize in any realistic model.

3. Higgs potential of order $(\phi^\dagger\phi)^5$

From Eqs. (1)–(2), the potential and the triple Higgs coupling in this case are

$$V(\phi,T) = \frac{m^2 + a_0 T^2}{2}(\phi^\dagger\phi) + \frac{\lambda}{4}(\phi^\dagger\phi)^2 + \frac{c_6}{8\Lambda^2}(\phi^\dagger\phi)^3 + \frac{c_8}{16\Lambda^4}(\phi^\dagger\phi)^4 + \frac{c_{10}}{32\Lambda^6}(\phi^\dagger\phi)^5, \quad (19)$$

$$\lambda_3 = \frac{3m_h^2}{v}\left(1 + \frac{2c_6 v^4}{m_h^2\Lambda^2} + \frac{4c_8 v^6}{m_h^2\Lambda^4} + \frac{5c_{10}v^8}{m_h^2\Lambda^6}\right). \quad (20)$$

Most of the analysis is the same as that for the $(\phi^\dagger\phi)^4$ case, and the extra minimum develops for $\phi > v$, when the correction to $\lambda_3^{\rm SM}$ is negative. Barring the possibility of metastability, the bound on the maximal negative correction corresponds to the point in which the extra minimum is degenerate with the physical one.

Figure 1(c) shows the possible modifications to $\lambda_3^{\rm SM}$ by viable Higgs potentials that obey the experimental constraints on the Higgs mass and the VEV. We see that for the cutoffs near 250 GeV, one can obtain variation in the λ_3 from $-5\lambda_5^{\rm SM}$ to $7\lambda_3^{\rm SM}$. Such large deviations make the triple Higgs coupling measurements at the LHC an exciting probe to the new physics. Figure 1(d) shows a subset of the region in the left panel, in which a SFOEPT can take place. The black and blue lines are retained from Figs. 1(a)–1(b) and serve as a reference for the comparison between the top and bottom rows.

In Figs. 1(c)–1(d) the orange regions correspond to $|c_6| = 1$, $|c_8| < 1$, $0 < c_{10} < 1$, the green region corresponds to $|c_6| < 1$, $|c_8| = 1$, $0 < c_{10} < 1$ and the purple region corresponds to $|c_6| < 1$, $|c_8| < 1$, $c_{10} = 1$. As expected, two clusters are observed in the orange and green regions corresponding to the sign flips of c_6 and c_8 respectively. As in the case of $(\phi^\dagger\phi)^4$, there is overlap between the regions. The green region is present beneath all the area occupied by the orange region, while the purple region is present beneath all the area occupied by the other two colors.

An interesting feature of this kind of potential is the presence of negative enhancements in Fig. 1(d) for the orange and green regions. This means that in principle there are regions of parameters in which a negative enhancement of λ_3 may be obtained consistently with a FOEPT. Figure 2 shows an example of the Higgs potentials, which is of order $(\phi^\dagger\phi)^5$, and satisfies the Higgs mass and the VEV constraints and also undergo a SFOEPT with large negative

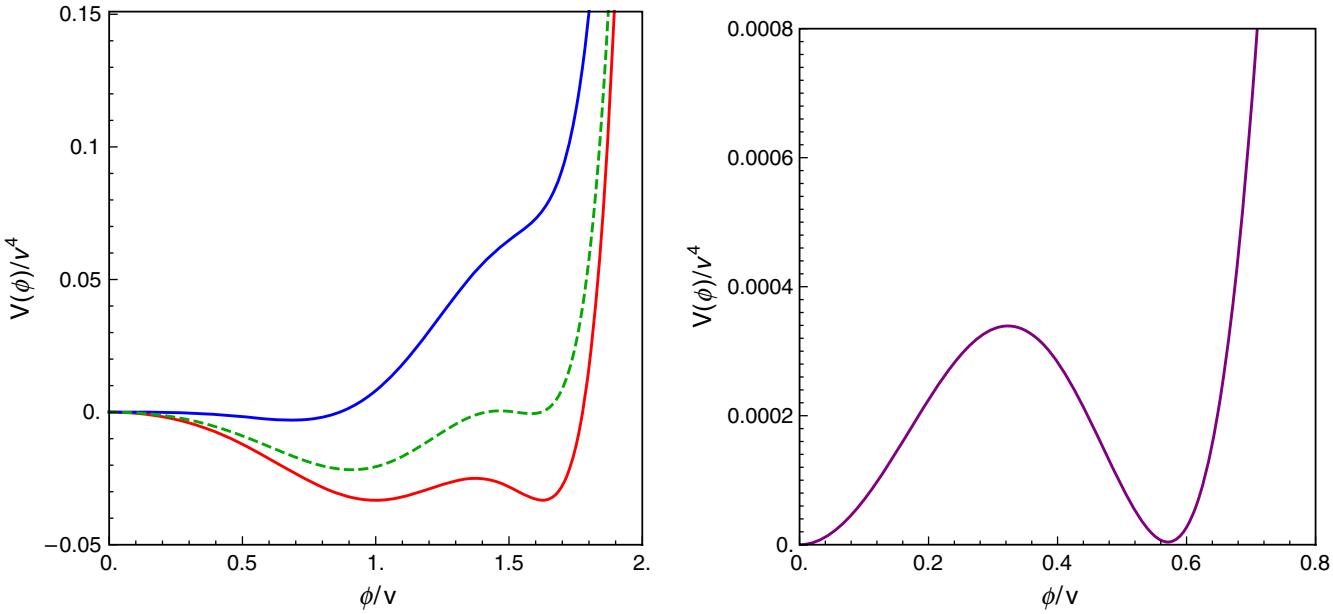

FIG. 2. Example of order $(\phi^\dagger\phi)^5$ potentials that correspond to the negative correction and also produce SFOEPT. In the left panel, the red line indicates the potential at $T = 0$, and the blue line corresponds to the temperature where the curvature at $\phi = 0$ is 0. The green line corresponds to the intermediate temperature of ~35 GeV. The purple curve on the right shows the potential at $T = T_c$. The coefficients $c_6 = 0.906$, $c_8 = -1$, $c_{10} = 0.346$, while $\Lambda \sim 263$ GeV, $T_c \sim 44$ GeV assuming $a_0 \sim 3$ as in the SM and $\delta = -1.23$.

enhancements of the triple Higgs coupling. In the left panel, the red line at the bottom corresponds to the potential at $T = 0$, while the blue line depicts the potential at $T = T_f$ that corresponds to the curvature at $\phi = 0$ being 0. The green (dashed) line represents an intermediate temperature. In the right panel, the purple curve shows the phase transition of the corresponding potential in the left panel at $T = T_c$. Let us stress that negative enhancements of the triple Higgs couplings are only consistent with a FOEPT for small values of the cutoff, $\Lambda \lesssim 350$ GeV. Hence, the correlation between the negative enhancements and the absence of a FOEPT remains generally valid.

III. MINIMAL EXTENSION WITH A SINGLET

Minimal extensions of the SM with just one singlet and their impact on electroweak baryogenesis have been studied in the literature [8,9,11,65–72]. Well-motivated UV complete scenarios such as the NMSSM also have an additional singlet, which can mix with the SM Higgs [6,73].

In Sec. III A we calculate the maximum enhancement of the triple Higgs coupling that can be allowed under the constraints of electroweak baryogenesis and the experimental constraints coming from the LHC. In Sec. III B we assume that the singlet is heavy and integrate it out giving rise to an EFT. The resultant expressions for the triple Higgs enhancement and bounds on the FOEPT region can be shown to be the same as those generated from the full Lagrangian in the small mixing angle limit. At the same time, this approach represents an example of the potentials discussed in the previous section and therefore allows one to discuss the validity and limitations of the effective theory approach.

A. Enhancement in the full scalar Lagrangian of the singlet extension

Consider a general scalar potential, with one-loop thermal correction only in the mass term, that can be written in a canonically normalized Lagrangian for the SM extended with one singlet field ϕ_s,

$$V(\phi_h,\phi_s,T) = \frac{m_0^2 + a_0 T^2}{2}\phi_h^2 + \frac{\lambda_h}{4}\phi_h^4 + a_{hs}\phi_s\phi_h^2 + \frac{\lambda_{hs}}{2}\phi_s^2\phi_h^2 + t_s\phi_s + \frac{m_s^2}{2}\phi_s^2 + \frac{a_s}{3}\phi_s^3 + \frac{\lambda_s}{4}\phi_s^4. \quad (21)$$

Here, ϕ_h is the Higgs field. The VEV for the Higgs field is $v = 246$ GeV. We assume that m_s is larger than the weak scale and we therefore ignore the very small temperature corrections affecting the singlet mass.

We stay in the limit where a_s and λ_s are much smaller compared to a_{hs} and λ_{hs} and drop the a_s and λ_s terms. This limit allows us to retain analytical control over the expressions for the mixing and triple Higgs coupling enhancement and to clearly demonstrate the connection with the EFT.[3] Within this approximation, the mass squared matrix in the basis $(\phi_h\phi_s)$ is

$$\mathcal{M}^2 = \begin{pmatrix} m_{11}^2 & m_{12}^2 \\ m_{21}^2 & m_{22}^2 \end{pmatrix} = \begin{pmatrix} 2\lambda_h v^2 & 2(a_{hs} + \lambda_{hs} v_s)v \\ 2(a_{hs} + \lambda_{hs} v_s)v & m_s^2 + \lambda_{hs} v^2 \end{pmatrix}, \quad (22)$$

where the VEV of the singlet field calculated at the Higgs vacuum is

$$v_s = -\frac{t_s + a_{hs} v^2}{m_s^2 + \lambda_{hs} v^2}. \quad (23)$$

The gauge eigenstate basis can be converted to the mass eigenstate basis as follows:

$$\phi_h = \cos\theta h_1 - \sin\theta h_2 + v, \quad (24)$$

$$\phi_s = \sin\theta h_1 + \cos\theta h_2 + v_s. \quad (25)$$

The mixing is given as

$$\tan 2\theta = \frac{4v(a_{hs} + \lambda_{hs} v_s)}{2\lambda_h v^2 - m_s^2 - \lambda_{hs} v^2} = \frac{4v(a_{hs} m_s^2 - t_s \lambda_{hs})}{(2\lambda_h v^2 - m_s^2 - \lambda_{hs} v^2)(m_s^2 + \lambda_{hs} v^2)}. \quad (26)$$

We use Eqs. (22) and (26) to convert the potential in Eq. (21) to the mass basis $(h_2 h_1)$ at the temperature $T = 0$, where h_1 is the lighter of the two scalar fields. The third derivative of the potential in Eq. (21) with respect to h_1 gives the triple Higgs coupling for the lower mass excitation as

$$\lambda_3 = 6\lambda_h v_h \cos^3\theta \left[1 + \left(\frac{\lambda_{hs} v_s + a_{hs}}{\lambda_h v_h}\right)\tan\theta + \frac{\lambda_{hs}}{\lambda_h}\tan^2\theta\right]. \quad (27)$$

In the limit of $v^2 \ll m_s^2$, one can easily show that the h_1 mass is given by

$$m_h^2 = 2\lambda_h v^2 - 4v^2 \frac{(a_{hs} m_s^2 - t_s \lambda_{hs})^2}{(m_s^2 + \lambda_{hs} v^2)^3}. \quad (28)$$

Using Eqs. (29), (28), and (26), we get

[3]The effects of a_s and λ_s on the triple Higgs coupling enhancement may be considered by performing an expansion in v/m_s [74].

$$\lambda_3 = \frac{3m_h^2}{v}\left[\cos^3\theta + \left(\frac{2\lambda_{hs}v^2}{m_h^2}\right)\sin^2\theta\cos\theta\right]. \quad (29)$$

For $\theta = 0$, we recover the SM result of $\lambda_3 = \frac{3m_h^2}{v}$.

In the small θ limit, the above formula reduces to

$$\lambda_3 = \frac{3m_h^2}{v}\left[1 + \left(\frac{2\lambda_{hs}v^2}{m_h^2} - \frac{3}{2}\right)\tan^2\theta\right]. \quad (30)$$

The same result can be recovered in the EFT approach by integrating out the heavier state as shown in Sec. III B. For the FOEPT in such a potential, we impose the following conditions:

$$V(0, T_c) = V(v_c, T_c), \qquad V'(v_c, T_c) = 0. \quad (31)$$

This leads to [6]

$$v_c^2 = \frac{1}{\lambda_{hs}}\left(-m_s^2 + \sqrt{\frac{2}{\lambda_h}}\left|m_s a_{hs} - \frac{\lambda_{hs}t_s}{m_s}\right|\right). \quad (32)$$

Here v_c is the value of the doublet scalar field at the critical temperature (T_c). The value of S is set to

$$v_{s,c} = -\frac{t_s + a_{hs}v_c^2}{m_s^2 + \lambda_{hs}v_c^2}, \quad (33)$$

which minimizes the potential at $\phi_h = v_c$. The constraints on the derivatives,

$$V'(\phi_c, T_c) = 0, \qquad V'(v, 0) = 0, \quad (34)$$

imply $a_0 T_c^2 = 8(F(v_c^2) - F(v^2))$. Here $F(\phi^2) = -\frac{V'(\phi,0)}{\phi}$ and $v = 246\,\text{GeV}$.

In Fig. 3 we show the enhancements of the trilinear couplings for different values of the singlet mass m_{singlet} and the quartic coupling λ_h. The orange region in Fig. 3 corresponds to the region consistent with a FOEPT, i.e. the boundaries correspond to $v_c^2 = 0$ and $T_c^2 = 0$.

From Eqs. (32) and (28), it follows that for $T_c = 0$, or equivalently $v_c = v$ one obtains

$$\tan^2\theta(v_c = v) \simeq \frac{m_h^2}{\lambda_{hs}v^2}. \quad (35)$$

Similarly, for $v_c = 0$, one obtains

$$\tan^2\theta(v_c = 0) \simeq \frac{m_h^2}{3\lambda_{hs}v^2}. \quad (36)$$

Using these expressions for small mixing angles, Eq. (30), one can easily show that

$$\delta(v_c = v) \simeq 2 - \frac{3m_h^2}{2\lambda_{hs}v^2} \quad (37)$$

while in the case of $v_c = 0$ one obtains

$$\delta(v_c = 0) \simeq \frac{2}{3} - \frac{m_h^2}{2\lambda_{hs}v^2}. \quad (38)$$

The region compatible with a FOEPT is always between these boundaries of $v_c = 0$ and $v_c = v$. Thus, the enhancement to the triple Higgs coupling is always less than 3, a result similar to the one obtained in the $(\phi^\dagger\phi)^3$ extension of the Higgs potential discussed in Sec. II A 1. Finally, let us mention that the SFOEPT constraint of $v_c > T_c$ [16] is almost always satisfied in the shown orange region.

In Fig. 3, we also show experimental constraints coming from Higgs physics and electroweak precision measurements. The mixing parameter $\sin^2\theta$ is denoted by the blue contours. The precision measurements of the SM-like Higgs properties at the LHC already impose strong constraints on the possible mixing angle of the singlet with the doublet. For example, the measurement of the Higgs production signal rates imposes an upper bound on $\sin^2\theta$. If one takes the gluon fusion production process, the combined measurement of ATLAS and CMS gives a signal strength [75]

$$\mu_{\text{ggF}} = 1.03^{+0.17}_{-0.15}. \quad (39)$$

When the other subleading processes, including the weak boson fusion, associated production and tth production are considered z, one obtains a combined signal strength

$$\mu = 1.09^{+0.11}_{-0.10}. \quad (40)$$

Since the mixing with a singlet leads to an overall decrease of all couplings to fermions and gauge bosons, the Higgs decay branching ratios are not affected and the signal strength is proportional to $\cos^2\theta$. Hence, from Eqs. (39)–(40) one obtains a 95% confidence level upper bound on $\sin^2\theta$, namely

$$\sin^2\theta < 0.27 \quad (41)$$

if only the more precisely measured gluon fusion processes are considered, and $\sin^2\theta < 0.11$ if the fit to all production processes is considered. In our work, we considered both bounds, as an indication of the constraints on the possible realization of this scenario.

In the case of small θ, as seen from Eq. (30), the correction to λ_3 compared to the SM is proportional to $\sin^2\theta$. From this, it is evident that the upper bound on the mixing is translated into an upper bound on the enhancement of λ_3,

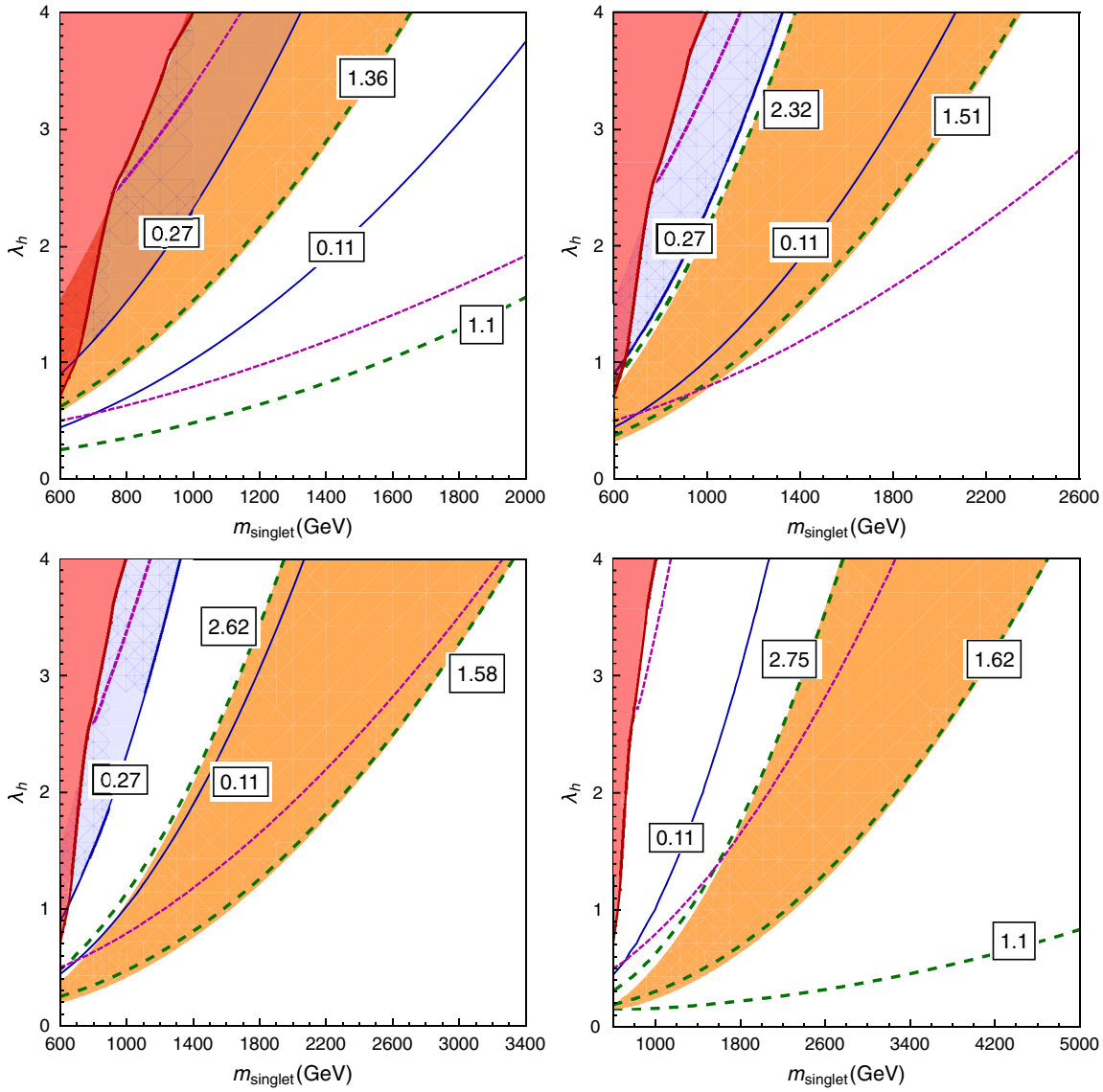

FIG. 3. Contours of the mixing parameter $\sin^2\theta$ (solid blue line) and of the enhancement of the triple Higgs coupling (dashed green line) given by Eq. (29) in the $m_{\text{singlet}} - \lambda_h$ plane. The blue shaded region denotes 2σ exclusion due to the gluon fusion channel. The orange shaded region represents the region consistent with a FOEPT. The region excluded up to 2σ confidence level by Higgs precision measurements is shaded in red. The constraints coming from m_W are shown by magenta (short-dashed) lines. In the top-left panel we present results for $\lambda_{hs} = 0.5$, while in the top-right, bottom-left and bottom-right panels we present results for $\lambda_{hs} = 1, 2, 4$ respectively.

$$\delta < \sin^2\theta_{\max}\left(\frac{2\lambda_{hs}v^2}{m_h^2} - \frac{3}{2}\right) \sim \sin^2\theta_{\max}\left(8\lambda_{hs} - \frac{3}{2}\right). \quad (42)$$

Hence, these constraints become more severe for smaller values of λ_{hs}.

From Eqs. (30) and (42), we also see that reducing λ_{hs} below $\frac{3m_h^2}{4v^2}$ leads to small negative values of δ. Therefore, a small suppression of the triple Higgs coupling with respect to the SM is viable for these values of λ_{hs}. As shown in Fig. 3, for these values of λ_{hs} the FOEPT region shifts rapidly to the higher mixing values and becomes unviable. Thus, there is trade-off between FOEPT and suppression of the triple Higgs coupling with respect to the SM as shown in the EFT case in the previous section.

Moreover, a light singlet that mixes with the SM Higgs will be produced at the LHC and may be searched for in various decay channels. This puts an additional constraint on the realization of this model, which is also shown in Fig. 3. The region to the left of the dark red solid line is excluded by the Higgs searches in the WW and ZZ channels [76].

The mixing between the doublet and the singlet is also constrained by precision W mass measurement [77,78]. The world average for the mass of the W boson is $m_W = 80.385 \pm 0.015$ GeV [79] including data from LEP II [80],

CDF [81] and D0 [82]. The prediction of the W mass is obtained by calculating the muon lifetime, which yields the relation,

$$m_W^2\left(1-\frac{m_W^2}{m_Z^2}\right)=\frac{\pi\alpha}{\sqrt{2}G_F}(1+\Delta r), \tag{43}$$

where Δr summarizes the radiative corrections. In the SM, in the on shell scheme, $m_W^{\rm SM}=80.361\pm0.007$ GeV [83,84],[4] which corresponds to $\Delta r^{\rm SM}=(37.979\pm 0.406)\times10^{-3}$, with the mass of the Higgs $m_h=125$ GeV. From Eq. (43), $\Delta r^{\rm exp}=(36.32\pm0.96)\times10^{-3}$, which is about 1.7σ from the SM value. Δr can be parametrized as

$$\Delta r=\Delta\alpha+\frac{c_w^2}{s_w^2}\left(\frac{\delta m_Z^2}{m_Z^2}-\frac{\delta m_W^2}{m_W^2}\right)+(\Delta r)_{\rm rem}, \tag{44}$$

where $\Delta\alpha$ is the radiative correction to the fine structure constant α, and c_w and s_w are the cosine and sine of the weak mixing angle. The second term is the on-shell self-energy correction to the gauge boson masses, which is well approximated by its value at zero momenta, and relates to the ρ parameter as $-\frac{c_w^2}{s_w^2}\Delta\rho$. The last term, $(\Delta r)_{\rm rem}$, includes vertex corrections and box diagrams at one-loop level, which are subleading. In the case of having a singlet mixed with the SM Higgs boson, Δr is given by

$$\Delta r=\Delta r^{\rm SM}-\frac{c_w^2}{s_w^2}(\Delta\rho^{\rm singlet}-\Delta\rho^{\rm SM}), \tag{45}$$

where $\Delta\rho^{\rm singlet}$ and $\Delta\rho^{\rm SM}$ are the $\Delta\rho$ calculated in the case with a mixed-in singlet and the SM [86].

$$\Delta\rho^{\rm singlet}-\Delta\rho^{\rm SM}=G_F\frac{m_Z^2}{2\sqrt{2}\pi^2}\sin^2\theta\left(H_T\left(\frac{m_{\rm Singlet}^2}{m_Z^2}\right)-H_T\left(\frac{m_h^2}{m_Z^2}\right)\right), \tag{46}$$

where

$$H_T(x)=\frac{3}{4}x\left(\frac{\log(x)}{1-x}-\frac{\log(x\times m_Z^2/m_W^2)}{1-x\times m_Z^2/m_W^2}\right). \tag{47}$$

The constraints on $\sin^2\theta$ obtained from the W mass become quite severe since as mentioned above, the SM is already in tension with the W mass measurement, and the singlet contribution increases this tension. The 2σ constraint coming from Δr calculated from Eq. (45) is shown by the lowered dashed magenta line in Fig. 3. On the other hand, if one assumes that some other new physics, which does not modify the loop induced Higgs production processes in a relevant way, is responsible for the difference between the SM and the current W mass measurement the bounds become significantly weaker as seen from the upper dashed magenta line in Fig. 3. It follows from Fig. 3 that even considering the tight constraints coming from Higgs measurements and precision electroweak parameters, a strongly first order phase transition is possible in these scenarios, provided $\lambda_{hs}\gtrsim1$. Large values of the singlet mass, of the order of the TeV scale, are possible in this case, making $\sin^2\theta$ small. In our analysis, we ignore the one-loop contributions to the effective potential since they are suppressed compared to the tree-level mixing effects. When λ_{hs} is sizable, as we show in the lower panels in Fig. 3, those corrections may not be negligible and should be taken into account in a more refined analysis of the critical parameters.

Before concentrating on the EFT analysis let us stress that an important contribution to the double Higgs production cross section that is always missed in this analysis is the resonant double Higgs production induced by the singlet. This can lead to a relevant contribution if the singlet is below the TeV scale and the mixing is sizable [87]. For instance, at the LHC with a center of mass energy of 14 TeV a 500 GeV singlet with a mixing of $\sin^2\theta=0.2$ will lead to a resonant production cross section through gluon fusion for the singlet of about 1.13 pb [88]. Under these conditions the branching ratio ${\rm BR}(S\to hh)\sim0.013$. Then the double Higgs production rate induced by the singlet is about 15 fb, which is about a factor of 4 smaller than the SM double Higgs production rate. Such a singlet would show up in the invariant mass distribution as a narrow resonance, as the singlet width is about 17 GeV. When the singlet gets heavier, say about 1 TeV, and for a mixing angle $\sin^2\theta=0.1$, the double Higgs production induced by the singlet is reduced to about 2.6 fb, which is significantly suppressed compared to the double Higgs production from the box and triangle diagrams, and difficult to detect in the standard decay channels. Then, in the region of a heavy singlet and small mixing angle, the EFT gives a proper description of the physics involved in double Higgs production. In this case, the singlet presence may only be inferred indirectly and one can make contact with an effective theory description of the modification of the trilinear couplings and of the double Higgs production rate.

B. EFT formulation for the singlet extension

In the limit of large values of the singlet mass m_s, and small mixing between the SM-like Higgs and the heavy singlet, we can integrate out the heavy singlet, and the resulting EFT should describe the same physics as we have described in the previous subsection.

[4] A calculation at the full two-loop level in the $\overline{\rm MS}$ scheme shows a value of $m_W=80.357\pm0.009\pm0.003$ GeV [85]. We stick to the on shell scheme calculation in our discussion, and the difference between the W mass calculation in both schemes would lead only to a minor change in our results.

For momenta very small compared to the masses of the scalars, solving the equation of motion for the singlet gives

$$\phi_s = -\frac{t_s + a_{hs}h^2}{m_s^2 + \lambda_{hs}h^2}. \tag{48}$$

Substituting this into the original potential in Eq. (21) yields an effective potential for h, which is given by [6]

$$V(h,T) = \frac{m^2(T)}{2}\phi_h^2 + \frac{\lambda_h}{4}\phi_h^4 - \frac{(t_s + a_{hs}\phi_h^2)^2}{2(m_s^2 + \lambda_{hs}\phi_h^2)}, \tag{49}$$

where $m^2(T) = m_0^2 + a_0T^2$. The integration out of the singlet also leads to a modification of the Higgs kinetic term, which means that the well-normalized Higgs field H will no longer be given by h, but will be affected by the mixing with the singlet. In other words, substituting the equation of motion of S in its kinetic term leads to an h dependent normalization factor,

$$\begin{aligned}&(\partial_\mu\phi_h)(\partial^\mu\phi_h) + (\partial_\mu\phi_s)(\partial^\mu\phi_s)\\ &\quad\to \left(1 + \frac{4\phi_h^2(a_{hs}m_s^2 - t_s\lambda_{hs})^2}{(m_s^2 + \lambda_{hs}\phi_h^2)^4}\right)(\partial_\mu\phi_h)(\partial^\mu\phi_h).\end{aligned} \tag{50}$$

Demanding that H is well normalized and retaining up to first order in the small parameter

$$z = \frac{(a_{hs}m_s^2 - t_s\lambda_{hs})^2 v^2}{m_s^8} \tag{51}$$

we obtain

$$\phi_H = \phi_h + \frac{2z\phi_h^3}{3v^2} + \mathcal{O}(\phi_h^5). \tag{52}$$

The corresponding c_H is

$$\frac{c_H}{4\Lambda^2} = \frac{z}{v^2}. \tag{53}$$

The variable z defined above is related to the mixing angle between the singlet and the doublet. From Eq. (26), we can write

$$\begin{aligned}\tan^2 2\theta &= \frac{16z}{(2\lambda_h y - 1 - \lambda_{hs}y)^2(1 + \lambda_{hs}y)^2}\\ &= 4\tan^2\theta + \mathcal{O}(\tan^3\theta).\end{aligned} \tag{54}$$

Substituting Eq. (61) and retaining first order in z we get

$$\begin{aligned}\tan^2 2\theta &= 16z + \mathcal{O}(z^2) = 4\tan^2\theta + \mathcal{O}(\tan^3\theta)\\ &\Rightarrow \tan^2\theta \sim 4z.\end{aligned} \tag{55}$$

From Eqs. (53), and (55), the constraint from the Higgs signal strength, Eq. (41), implies that c_H tends to be small, namely

$$\frac{c_H v^2}{\Lambda^2} < 0.37. \tag{56}$$

Inverting the relation between ϕ_h and ϕ_H given in Eq. (52) one obtains

$$\phi_h = \phi_H - \frac{2z}{3v^2}\phi_H^3 + \mathcal{O}(\phi_H^5). \tag{57}$$

Substituting this in Eq. (49), we get an effective potential, which retaining up to order H^6 corrections is given by

$$\begin{aligned}V_{\rm eff}(\phi_H,T) = \frac{m^2}{2}\phi_H^2 + \left(\frac{\lambda_h - 2z/y}{4} - \frac{2m^2 z}{3v^2}\right)\phi_H^4\\ + \left(\frac{-4z(\lambda_h - 2z/y) + 3z\lambda_{hs}}{6v^2}\right)\phi_H^6,\end{aligned} \tag{58}$$

where $y = v^2/m_s^2$. This shows the presence of a large negative correction to the quartic coupling, of order $2z/y$. This correction, which depends only on ratios of mass parameters, allows for the presence of a negative effective quartic coupling which, according to our analysis of the EFT at this order in Sec. II A 1, is essential for the obtention of a FOEPT.

Using this potential Eq. (49) we apply the Higgs mass condition to write

$$\left(V''_{\rm eff} - \frac{V'_{\rm eff}}{\phi_H}\right)\Big|_{\phi_H=\langle\phi_H\rangle} = m_H^2, \quad \text{where } \langle\phi_H\rangle = v + \frac{2zv}{3}. \tag{59}$$

Solving this simultaneously with

$$\frac{V'_{\rm eff}}{\phi_H}\Big|_{\phi_H=\langle\phi_H\rangle} = 0 \tag{60}$$

leads to a relation of the value of λ and the Higgs mass,

$$\lambda = \lambda_h - \frac{2z}{y} = \frac{m_H^2}{2v^2} + \left(\frac{2m_H^2}{v^2} - 6\lambda_{hs}\right)z. \tag{61}$$

Since $m_H^2/(2v^2) \simeq 1/8$, for small values of z the coefficient of the quartic coupling λ is small in magnitude and may be negative for λ_{hs} of order 1.

Moreover, a sizable correction to the sixth order term appears, which is there even in the absence of kinetic term corrections. Observe that $\lambda_h - 2z/y$, which as shown above

corresponds to λ in the EFT analysis, appears also in the first term in the ϕ_H^6 coefficient. Since λ is small as discussed above, the ϕ_H^6 coefficient is dominated by the second term in the bracket. The cutoff scale can be then calculated from

$$\frac{c_6}{8\Lambda^2} \sim \frac{3\lambda_{hs} z}{6v^2} = \frac{\lambda_{hs}(am_s^2 - t_s\lambda_{hs})^2}{2m_s^8}. \tag{62}$$

The corresponding cutoff scale is, for $c_6 = 1$,

$$\Lambda^2 = \frac{m_s^8}{4\lambda_{hs}(am_s^2 - t_s\lambda_{hs})^2}. \tag{63}$$

Thus, when $(am_s^2 - t\lambda_{hs})$ and λ_{hs} become sizable, Λ could be significantly lower than m_s. However, $am_s^2 - t\lambda_{hs}$ is related to $\sin^2\theta$, which is constrained by electroweak symmetry breaking, precision Higgs measurements, heavy SM-like Higgs searches, and W mass as discussed above; the cutoff scale cannot be lowered arbitrarily. For example, since λ is small, from Eq. (61), we have

$$\lambda_h \sim \frac{2z}{y} = \frac{2(am_s^2 - t_s\lambda_{hs})^2}{m_s^6}. \tag{64}$$

Then the cutoff scale is about

$$\Lambda^2 \sim \frac{m_s^2}{2\lambda_h\lambda_{hs}}. \tag{65}$$

It is instructive to compare these results with those shown in Fig. 3. For instance, when m_{singlet} is about 1.4 TeV, $\lambda_{hs} = 2$, and $\lambda_h = 2$, that is close to the boundary of the orange region in the bottom-left panel of Fig. 3, the cutoff scale is about 494 GeV, which is about the lower bound of the cutoff scale in a $(\phi^\dagger\phi)^3$ theory and is consistent with the left boundary of the orange region in this figure. Similarly, for the same results of λ_h and λ_{hs}, and for $m_{\text{singlet}} = 2.4$ TeV, that is closed to the other boundary in the bottom-left panel of Fig. 3, the effective cutoff scale that is obtained from Eq. (65) is about 848 GeV that is very close to the upper bound on Λ that is obtained for a FOEPT in the $(\phi^\dagger\phi)^3$ extension. One can check that similar values of the cutoff are obtained at the left and right boundaries of the orange regions in Fig. 3 for other values of λ_h, λ_{hs} and m_{singlet}.

After substituting Eq. (61) and considering the field fluctuations of the field ϕ_H,

$$\phi_H = v_H + H, \tag{66}$$

we obtain

$$\lambda_3 \equiv g_{HHH} = \frac{3m_H^2}{v}\left(1 + 4z\left(\frac{2\lambda_{hs}v^2}{m_H^2} - \frac{3}{2}\right)\right). \tag{67}$$

Using Eqs. (67) and (55) we obtain

$$\lambda_3 = \frac{3m_H^2}{v}\left(1 + \left(\frac{2\lambda_{hs}v^2}{m_h^2} - \frac{3}{2}\right)\tan^2\theta\right). \tag{68}$$

This formula is the same as that obtained in Eq. (30) from the small mixing limit of the enhancement up to $\tan^2\theta$ order in the full renormalizable Lagrangian. Thus, as expected, the EFT approach is equivalent to the small mixing limit of the full theory. To make the analogy more transparent let us emphasize that from Eq. (57) the fluctuations of the field $\phi_h = v + h$ and H are related by

$$h = \left(1 - \frac{\tan^2\theta}{2}\right)H \simeq \cos\theta H. \tag{69}$$

That is the same relation we obtain between h_1 and h in the full theory, Eq. (24), when we consider negligible h_2 fluctuations associated with its decoupling from the low energy theory.

We note that the effective potential derived in Eq. (58) is of order ϕ_H^6. This is the same order as the $(\phi^\dagger\phi)^3$ potential described in Sec. II A 1. In this case, however, the range of values of δ is not constrained from 2/3 to 2 as expected from the $(\phi^\dagger\phi)^3$ theory, but is shifted to lower values. This is due to the kinetic term corrections we did not consider in the analysis in Sec. II. For $\lambda_{hs} \gtrsim 1$, the kinetic term corrections remain significantly smaller than the ones associated with the effective potential modification, which are controlled by the λ_{hs} coupling. Expressing Eq. (67) in terms of c_6 and c_H, using Eqs. (62) and (53), we obtain

$$\lambda_3 = \frac{3m_H^2}{v}\left(1 + c_6\frac{2v^4}{m_h^2\Lambda^2} - \frac{3}{2}c_H\frac{v^2}{\Lambda^2}\right). \tag{70}$$

This is consistent with Eq. (6) when $c_H = 0$. Also, this is consistent with Eq. (34) in Ref. [65] and Eq. (124) of Ref. [89] when taking $\lambda = m_h^2/(2v^2)$. It is worth noticing that Eq. (70) is suitable for the study of the region of parameters consistent with a FOEPT while Eq. (34) in Ref. [65] and Eq. (124) in Ref. [89] are only valid in the region where λ can be approximated as $m_h^2/(2v^2)$. As mentioned in Sec. II A, it has been overlooked in Ref. [65] that in the region consistent with a FOEPT, λ is small and negative, and the proper relation between λ and the Higgs mass can only be obtained after including the higher order corrections proportional to c_6, Eq. (9), and therefore $\lambda = m_h^2/(2v^2)$ is no longer a valid approximation in this region.

Higher powers of ϕ_H in Eq. (58) can be obtained by retaining more terms in the expansions with respect to z and

y variables. For instance, we have checked that at next order the well-normalized field is given by

$$\phi_H = \phi_h + \frac{2z\phi_h^3}{3v^2} - \frac{2(z^2+4yz\lambda_{hs})\phi_h^5}{5v^4}. \quad (71)$$

Expressing h in terms of H,

$$\phi_h = \phi_H - \frac{2z\phi_H^3}{3v^2} + \frac{2(13z^2+12yz\lambda_{hs})\phi_H^5}{15v^4}, \quad (72)$$

one can obtain the value of δ, as we did below, that is given by

$$\delta = \left(-6+\frac{8v^2\lambda_{hs}}{m_h^2}\right)z + \left(30-\frac{48v^2\lambda_{hs}}{m_h^2}\right)z^2 + \left(40\lambda_{hs}-\frac{32v^2\lambda_{hs}^2}{m_h^2}\right)yz. \quad (73)$$

That indeed reproduces the small θ expansion of the exact formula, Eq. (30).

Again, it is straightforward to see that H and h are related by

$$h = \left(1-\frac{\tan^2\theta}{2}+\frac{3\tan^4\theta}{8}\right)H \simeq \cos\theta H \quad (74)$$

as expected from the relation between h_1 and h in the full theory, Eq. (24).

Before we concentrate on collider phenomenology, let us comment on the negative enhancement in a theory with a mixed-in singlet. Once a small singlet quartic coupling λ_s is turned on to stabilize the potential, λ_{hs} can go to negative values, as long as $|\lambda_{hs}| < \sqrt{\lambda_h\lambda_s}$. A small λ_s leads to a contribution to λ_3 suppressed by $\sin^3\theta$, $\sim 6\lambda_s v_s \sin^3\theta$. As seen in Eq. (68), a negative λ_{hs} provokes a negative enhancement while a small positive λ_s adds negligible contribution to λ_3. We note that, in the EFT context, the λ_s term generates a term of order $\frac{1}{4}\lambda_s\frac{a_{hs}^4}{ms^8}H^8$ in the effective potential, and allows for the terms of order of H^6 negative. Therefore, a theory with a negative λ_{hs} may result in a negative enhancement in λ_3 as we go beyond a $(\phi^\dagger\phi)^3$ theory described before, as shown for instance in the green region in Fig. 1.

IV. MEASUREMENT OF THE TRIPLE HIGGS COUPLING AT THE LHC

The triple Higgs coupling λ_3 can be probed by the double Higgs production at the LHC. At the leading order (LO), there are two diagrams contributing to the process: the triangle diagram, which is sensitive to λ_3, and the box diagram. The two diagrams interfere with each other destructively. The LO matrix elements of the subprocess are known [90–92]. NLO QCD corrections are known [93] in an EFT approach, by applying the low energy theorem (LET) [94] within the infinite quark mass approximation. Next-to-next-to-leading order (NNLO) corrections in the large quark mass limit are calculated in [95–97]. Next-to-next-to-leading logarithmic (NNLL) corrections are calculated in [98,99]. For our analysis, we take a NNLO K-factor = 2.27 [95].

For our analysis, we assume the double Higgs production is modified because of the altered λ_3 coupling. The double Higgs production rate could also be modified by introducing new particles that couple to the gluon, and the Higgs in the loop [100,101]. Those new particles change the amplitudes corresponding to the triangle diagram and the box diagram at the same time and also contribute to the single Higgs production, which is well measured at the LHC. Therefore, those contributions are constrained and tend to be small for the double Higgs production [101].

For the Higgs decays, we consider $\gamma\gamma$, $\tau^+\tau^-$, W^+W^- and $b\bar{b}$ modes, which are measured in the single Higgs production at the LHC. The production rate of double Higgs is suppressed by three orders of magnitude compared to the single Higgs production at the LHC [88], so one of the two Higgs bosons needs to decay to $b\bar{b}$ for statistics, and $\gamma\gamma$, $\tau^+\tau^-$, and W^+W^- modes can be considered for the other Higgs boson. We do not study the $b\bar{b}W^+W^-$ decay mode due to the overwhelming $t\bar{t}$ background that renders a low significance [28,29]. The four b final states suffer from a large QCD background and therefore are very difficult for the LHC even in the boosted region of the Higgs boson, where the jet substructure techniques may be used [28]. In this work, we therefore focus on the $b\bar{b}\gamma\gamma$ mode.

The irreducible background in the $hh \to b\bar{b}\gamma\gamma$ channel includes $b\bar{b}\gamma\gamma$, $t\bar{t}h(\gamma\gamma)$ and $Z(b\bar{b})h(\gamma\gamma)$ processes. Considering the possibility that a charm or light quarks fake a bottom quark, and a light jet fakes a photon, the processes $c\bar{c}\gamma\gamma$, $jj\gamma\gamma$, and $b\gamma jj$ also contribute to the background. The $t\bar{t}h$ background can be efficiently suppressed by vetoing extra jets, leptons or missing energy. Requiring the invariant mass of the two b-jets, $m_{b\bar{b}}$ and the two photons, $m_{\gamma\gamma}$ within some window of the Higgs mass helps to reduce the Zh background and the QCD background. In the previous studies, a cut on the invariant mass of the two Higgs bosons, m_{hh} [29,31,33], or some equivalent cuts were required [34] to be imposed to further reject the background. In those studies, it was shown that an $O(1)$ precision in the triple Higgs boson coupling λ_3 may be achieved at the 14 TeV run of the LHC, with a high integrated luminosity of order 3000 fb^{-1}.

As pointed out in [31], and also noticed in [34], the acceptance of new physics with large λ_3 compared to the SM value is much lower for the same set of cuts. The reason for this behavior is that the m_{hh} distribution is very different for the SM and for new physics with a large λ_3. When m_{hh} is below the $2m_t$ threshold, there are only real parts of the triangle and the box diagram, and these two diagrams

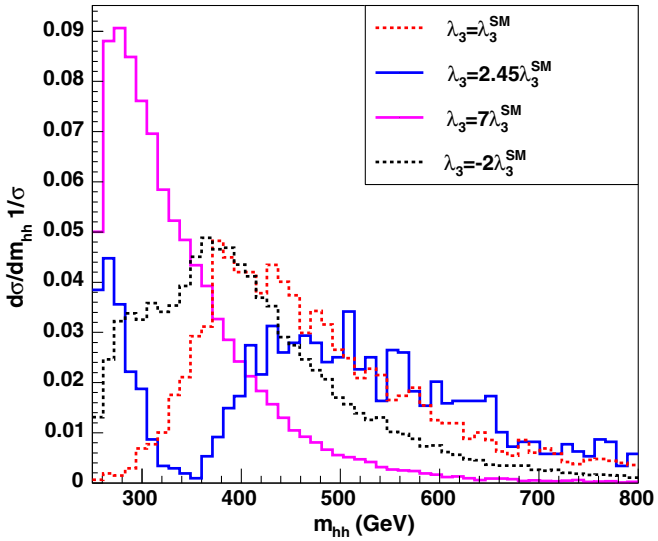

FIG. 4. Normalized m_{hh} distributions for $\lambda_3 = \lambda_3^{\rm SM}$, $\lambda_3 = 2.45\lambda_3^{\rm SM}$ and $\lambda_3 = 7\lambda_3^{\rm SM}$ and $\lambda_3 = -2\lambda_3^{\rm SM}$. The cancellation between the box and triangle diagram is exact at $\lambda_3 = 2.45\lambda_3^{\rm SM}$ at $2m_t$ threshold, which explains the dip. Note that the distribution shifts to smaller values as λ_3 increases.

interfere with each other destructively. The cancellation is exact at the $2m_t$ threshold at $\lambda_3 = 2.45\lambda_3^{\rm SM}$. When m_{hh} is above the $2m_t$ threshold, imaginary parts start to develop, and the destructive interference is not as strong as it is below the $2m_t$ threshold. So as λ_3 increases, the cross section increases more significantly below the $2m_t$ threshold than above the $2m_t$ threshold. This means that, as λ_3 increases, the distribution of m_{hh} shifts to smaller values, as shown in Fig. 4, where we plot the normalized m_{hh} distribution using MCFM [102] for various values of λ_3. Thus, using the same set of cuts for new physics with a large λ_3 leads to a low acceptance at the LHC. Therefore, a modified cut on m_{hh}, $m_{hh} < 2m_t$ should be used when searching for new physics with a large λ_3.

The m_{hh} distribution also helps to distinguish positive and negative values of λ_3. For negative λ_3, the m_{hh} distribution shifts to larger values compared to the positive λ_3 that yields the same production for gluon fusion because of the constructive interference between the box and the triangle diagrams, as shown in Fig. 4. Then, the negative and positive values of λ_3 that have the same total rate of gluon fusion can be distinguished by studying the m_{hh} distribution.

A. Double Higgs production in the $b\bar{b}\gamma\gamma$ channel

In order to understand the impact of the cuts in the m_{hh} invariant mass distribution on the reach for double Higgs production at the LHC and future colliders, we have performed a collider study of this process for different values of the triple Higgs coupling and in different Higgs decay channels. In spite of the low rate, one of the most sensitive channels is when the Higgs decays into photons, since it allows a good Higgs reconstruction with relatively low background. We therefore performed a collider study for the $hh \to b\bar{b}\gamma\gamma$ channel. The signal with various values of λ_3 is generated by MCFM [102], passed to Pythia8 [103] for parton shower and hadronization, and then passed to Delphes [104] for detector simulation. We apply a NNLO K-factor of about 2.27 for the signal [95]. The background processes are generated with MadGraph [105] and then passed to Pythia and Delphes. We apply a NLO K-factor = 1.1 for $t\bar{t}h$ and a NNLO QCD, NLO EW K-factor = 1.33 for Zh [88]. There are no higher order corrections known for the QCD backgrounds, and therefore, all the QCD processes are normalized to LO. We take a b-tagging efficiency of 70% and a mistag rate of 24% for c-jets and 2% for light jets [106]. We adopt a photon tagging rate of 85% and a jet to photon fake rate $\epsilon_{j\to\gamma} = 1.2 \times 10^{-4}$ [107]. We require the following cuts:

$$\begin{aligned} p_t(b) &> 30\ \text{GeV}, \qquad |\eta(b)| < 2.5, \\ p_t(\gamma) &> 30\ \text{GeV}, \qquad |\eta(\gamma)| < 2.5 \\ 112.5\ \text{GeV} &< m_{bb} < 137.5\ \text{GeV}, \\ 120\ \text{GeV} &< m_{\gamma\gamma} < 130\ \text{GeV}. \end{aligned} \tag{75}$$

For the SM case, we further require

$$m_{hh} > 350\ \text{GeV}, \tag{76}$$

while for $\lambda_3 > 3\lambda_3^{\rm SM}$, we require

$$250\ \text{GeV} < m_{hh} < 350\ \text{GeV}. \tag{77}$$

The results for LHC 14 TeV are displayed in Table I. As shown in Table II, the significance reaches 5σ level at $\lambda_3 \sim 6.5\lambda_3^{\rm SM}$, and $\lambda_3 \sim -0.2\lambda_3^{\rm SM}$ at 14 TeV and 3000 fb^{-1}. One caveat of this analysis is that we include a K-factor for the signal (and also for the ZH and tth background), but the QCD background is only considered at LO. If we assume a K-factor of about 2 for the QCD processes, the significance drops by a factor of $\sqrt{2}$, which can be compensated by the fact that there are two detectors.

It is instructive to compare these results with those obtained by the LHC experimental collaborations. ATLAS and CMS have performed similar studies on the $hh \to bb\gamma\gamma$ channel. For HL-LHC, ATLAS expects a 1.3σ significance for the SM case [34], and the CMS expectation is about 1.6σ [108]. These results are about a factor two weaker than the ones we obtain in our study. On the other hand, the results from current theoretical studies show a significance range from 2σ to 6σ [27,29,31,33]. The difference with the experimental results may proceed from different sources. In our analysis, we use very simple cuts, and we do not attempt to optimize the cuts for the SM background, but we believe extra cuts do not help much in this case as it is a rare

TABLE I. Cross section in fb of the hh signal and various backgrounds expected at the LHC at $\sqrt{s} = 14$ TeV after applying the cuts discussed in Eqs. (75)–(77).

	σ (fb)	Eq. (75) + Eq. (76) (fb)	Eq. (75) + Eq. (77) (fb)
$hh(b\bar{b}\gamma\gamma)$ $(\lambda_3 = \lambda_3^{\rm SM})$	0.15	1.0×10^{-2}	⋯
$hh(b\bar{b}\gamma\gamma)$ $(\lambda_3 = 5\lambda_3^{\rm SM})$	0.26	⋯	1.12×10^{-2}
$hh(b\bar{b}\gamma\gamma)$ $(\lambda_3 = 7\ \lambda_3^{\rm SM})$	0.71	⋯	3.3×10^{-2}
$hh(b\bar{b}\gamma\gamma)$ $(\lambda_3 = 9\ \lambda_3^{\rm SM})$	1.43	⋯	6.08×10^{-2}
$hh(b\bar{b}\gamma\gamma)$ $(\lambda_3 = 0)$	0.29	1.33×10^{-2}	⋯
$hh(b\bar{b}\gamma\gamma)$ $(\lambda_3 = -\lambda_3^{\rm SM})$	0.50	2.26×10^{-2}	⋯
$hh(b\bar{b}\gamma\gamma)$ $(\lambda_3 = -2\lambda_3^{\rm SM})$	0.77	2.94×10^{-2}	⋯
$b\bar{b}\gamma\gamma$	5.05×10^{3}	1.34×10^{-2}	4.0×10^{-2}
$c\bar{c}\gamma\gamma$	6.55×10^{3}	4.19×10^{-3}	2.68×10^{-2}
$b\bar{b}\gamma j$	9.66×10^{6}	4.60×10^{-3}	1.38×10^{-2}
$jj\gamma\gamma$	7.82×10^{5}	2.38×10^{-3}	5.26×10^{-3}
$t\bar{t}h$	1.39	1.40×10^{-3}	2.33×10^{-3}
zh	0.33	6.86×10^{-4}	9.01×10^{-4}
$b\bar{b}jj$	7.51×10^{9}	5.34×10^{-4}	6.47×10^{-4}

process. We also do not try to perform a realistic detector simulation.

The main issue we stress is the impact of the cuts in the invariant mass distribution when studying possible modifications of the triple Higgs coupling. We obtain a very significant sensitivity improvement in the case where λ_3 deviates significantly from the SM; when we implement the new cuts in Eq. (77) we propose such cases. For instance, when $\lambda_3 = 5\lambda_3^{\rm SM}$, if we use the cuts in Eq. (76), we only expect a 0.67σ significance, while we expect 2.1σ significance if we use the cuts in Eq. (77). Similar large improvements are obtained for other sizable values of $\lambda_3 > 3\lambda_3^{\rm SM}$.

Due to the relatively low sensitivity of the LHC in looking for double Higgs production, it is interesting to consider similar signatures at future colliders, in particular, a future high energy pp collider. The sensitivity will depend on many factors, including the center of mass energy and the detector performance. To be specific, we consider the case of a 100 TeV pp collider, assuming that the detector performance stays the same as at the LHC, performing similar cuts as the ones in the LHC analysis. We show the results in Tables III–IV. In our analysis, we considered only positive values of λ_3, since as shown above, the LHC is already sensitive to the negative values. It is then easy to extrapolate the same analysis for higher energies. The results presented in Table III show that a 100 TeV collider should be sensitive to triple Higgs boson couplings $\lambda_3 \sim 5\lambda_3^{\rm SM}$, where the same cuts proposed in Eq. (75) were used. The significance we obtain is similar to the ones obtained in Refs. [13] and [109] for the same process. Again, we obtain a significant improvement of the sensitivity at large values of $\lambda_3 > 3\lambda_3^{\rm SM}$ when the new cuts on m_{hh} given in Eq. (77) are used.

TABLE II. Significance expected for hh at the LHC at $\sqrt{s} = 14$ TeV for an integrated luminosity of 3000 fb^{-1} after applying cuts in Eq. (75) + Eq. (76) ($\lambda_3 < 3\lambda_3^{\rm SM}$), or Eq. (75) + Eq. (77) ($\lambda_3 > 3\lambda_3^{\rm SM}$).

λ_3	$\lambda_3^{\rm SM}$	$5\lambda_3^{\rm SM}$	$7\lambda_3^{\rm SM}$	$9\lambda_3^{\rm SM}$	0	$-\lambda_3^{\rm SM}$	$-2\lambda_3^{\rm SM}$
$S/\sqrt{B}$	3.3	2.1	6.0	11	4.4	7.5	9.8

TABLE III. Cross section of the hh signal and various backgrounds expected at a 100 TeV collider after applying the cuts discussed in Eqs. (75)–(77).

	σ (fb)	Eq (75) + Eq (76) (fb)	Eq (75) + Eq (77) (fb)
$hh(\lambda_3 = \lambda_3^{\rm SM})$	3.4	0.11	⋯
$hh(\lambda_3 = 3\lambda_3^{\rm SM})$	1.48	0.042	⋯
$hh(\lambda_3 = 5\lambda_3^{\rm SM})$	4.45	⋯	0.10
$b\bar{b}\gamma\gamma$	1.7×10^{6}	0.129	0.52
$c\bar{c}\gamma\gamma$	1.0×10^{5}	6.45×10^{-2}	0.42
$b\bar{b}\gamma j$	1.19×10^{5}	1.68×10^{-2}	6.72×10^{-2}
$jj\gamma\gamma$	2.73×10^{6}	1.92×10^{-2}	7.3×10^{-2}
$t\bar{t}h$	86.41	2.72×10^{-2}	2.53×10^{-2}
zh	0.88	1.76×10^{-3}	1.4×10^{-3}
$b\bar{b}jj$	4.07×10^{10}	2×10^{-3}	4.7×10^{-3}

TABLE IV. The significance of double Higgs production expected for hh at a 100 TeV collider for an integrated luminosity of 3000 fb^{-1} after applying cuts in Eq. (75) + Eq. (76) ($\lambda_3 < 3\lambda_3^{\rm SM}$), or Eq. (75) + Eq. (77) ($\lambda_3 > 3\lambda_3^{\rm SM}$).

λ_3	$\lambda_3^{\rm SM}$	$3\lambda_3^{\rm SM}$	$5\lambda_3^{\rm SM}$
$S/\sqrt{B}$	11	4.5	5.3

B. Double Higgs production in the $b\bar{b}\tau^+\tau^-$ channel

Since the Higgs has many different significant decay channels, it is useful to think about double Higgs production in channels different from the $bb\gamma\gamma$ considered in this work. A particularly interesting one is the $bb\tau\tau$ channel. The $b\bar{b}\tau^+\tau^-$ channel enjoys a larger cross section but suffers from the difficulty in the event reconstruction due to the missing energy associated with τ decays. It also suffers from larger backgrounds that should be properly considered to obtain a realistic reach estimate.

The τ pair invariant mass $m_{\tau\tau}$ may be estimated by the missing mass calculator [110], and similar methods could be used to estimate m_{hh} in this channel. In order to estimate the reach in this channel, we assume that the $m_{\tau\tau}$ invariant

mass can be reconstructed with a similar resolution as m_{bb} [110] invariant mass. Furthermore, we assume that the two Higgs invariant mass m_{hh} can be reconstructed as well as it is obtained at the parton level. The discovery reach is then estimated adopting the cuts and background calculations presented in Ref. [29].

We go beyond the analysis of Ref. [29] by including the relevant background coming from the $bbjj$ process. Under the above conditions, and assuming a jet to τ fake rate $\epsilon_{j\to\tau} = 1/100$ [31], we obtain a significance $S/\sqrt{B} \sim 3.75$ for $\lambda_3 = \lambda_3^{\rm SM}$ that is similar to the one obtained in the $\gamma\gamma$ channel. However, estimating m_{hh} in the $bb\tau\tau$ channel is very difficult. For that reason, CMS preforms a preliminary study using the Stransverse mass m_{T2} instead of m_{hh} to distinguish the signal from the background, and shows a 0.9σ significance for HL-LHC [108]. That is significantly smaller than the one found in [32] using a similar method. Therefore, the $bb\tau\tau$ channel may represent a good complementary channel to the $bb\gamma\gamma$ one, and should be studied further.

V. CONCLUSIONS

In this work, we have studied the modifications of the triple Higgs couplings in theories in which the Higgs potential is modified by the addition of higher order, nonrenormalizable operators, induced by the presence of new physics at the weak scale. Contrary to previous statements in the literature, we have shown that a simple addition of a dimension-6 operator may lead to a large modification of the triple Higgs coupling λ_3 with respect to its SM value in the regions of parameter space consistent with a FOEPT.

Furthermore, the addition of higher order operators may also lead to a reduction of the triple Higgs coupling, or even its change of sign, with relevant implications for collider physics. Interestingly, negative enhancements of the triple Higgs coupling tend to be associated with a second order phase transition, while a first order phase transition tends to be associated with a large positive enhancement of this coupling.

We also argue, building on the previous results in the literature, that different values of the triple Higgs coupling will have a strong impact not only on the total cross section, but also on the invariant mass distribution of double Higgs production at the LHC. This motivates the use of different cuts for double Higgs production for values of the trilinear coupling about or smaller than the SM value than for the large values of λ_3. The determination of the total cross section, together with the analysis of the invariant mass distribution, may give hints not only about the magnitude of the departure of the Higgs coupling with respect to the SM value, but also of its sign. Considering these different cuts in the invariant mass distribution and including background processes that were previously ignored in the literature, we showed that at the 14 TeV run of the LHC at high luminosities, a significance of order of 3.3σ is expected for $\lambda_3 = \lambda_3^{\rm SM}$, and a 5σ significance is expected for $\lambda_3 = 6.5\lambda_3^{\rm SM}$ ($-0.2\lambda_3^{\rm SM}$) for the $b\bar{b}\gamma\gamma$ channel. The $b\bar{b}\tau^+\tau^-$ channel presents a promising complementary channel.

ACKNOWLEDGMENTS

We thank V. Barger, L. Everett, J. Gao, H. Haber, A. Ismail, I. Lewis, M. Peskin and L. T. Wang for useful discussions. Work is supported by the U.S. Department of Energy under Award No. DE-FG02-13ER41958. Work at ANL is supported in part by the U.S. Department of Energy under Award No. DE-AC02-06CH11357. P. H. is partially supported by U.S. Department of Energy Award No. DE-FG02-04ER41286.

APPENDIX A: TRIPLE HIGGS COUPLING

We add tree-level nonrenormalizable operators to the Higgs potential to get the most general effective potential at the tree level

$$V(\phi) = \sum_{n=1}^{\infty} \frac{k_{2n}}{2n}\phi^{2n}, \tag{A1}$$

where $k_2 = m^2$, $k_4 = \lambda$ and, for $n \geq 3$,

$$\frac{k_{2n}}{2n} = \frac{c_{2n}}{2^n \Lambda^{2(n-2)}}. \tag{A2}$$

For the potential to have a minimum at the VEV it must satisfy

$$\left.\frac{\partial V}{\partial \phi}\right|_{\phi=v} = \sum_{n=1}^{\infty} k_{2n} v^{2n-1} = 0. \tag{A3}$$

The second derivative at the VEV must be the square of the Higgs boson mass as discovered by the CMS and ATLAS experiments at the LHC [111,112],

$$\begin{aligned} \frac{\partial^2 V}{\partial \phi^2} &= \sum_{n=1}^{\infty} (2n-1) k_{2n} \phi^{2n-2}, \\ \left.\frac{\partial^2 V}{\partial \phi^2}\right|_{\phi=v} &= \sum_{n=1}^{\infty} (2n-1) k_{2n} v^{2n-2} = m_h^2. \end{aligned} \tag{A4}$$

Dividing Eq. (A3) by v and then subtracting it from Eq. (A4), we get

$$\sum_{n=2}^{\infty} (n-1) k_{2n} v^{2n-4} = \frac{m_h^2}{2v^2}. \tag{A5}$$

The third derivative gives the triple Higgs coupling as we are already in the canonical normalization, where we can substitute $\phi = h + v$ and $v = 246$ GeV,

$$\left.\frac{\partial^3 V}{\partial \phi^3}\right|_{\phi=v} = \sum_{n=2}^{\infty}(2n-1)(2n-2)k_{2n}v^{2n-3}. \quad \text{(A6)}$$

Multiplying Eq. (A5) by $6v$ and subtracting it from Eq. (A6) we get

$$\lambda_3 = \left.\frac{\partial^3 V}{\partial \phi^3}\right|_{\phi=v} = \frac{3m_h^2}{v}\left(1 + \sum_{n=3}^{\infty}\frac{4(n-1)(n-2)k_{2n}v^{2(n-1)}}{3m_h^2}\right). \quad \text{(A7)}$$

Substituting for k in terms of the cutoff of the effective theory (Λ) and the corresponding dimensionless coefficients (c_{2n}) from Eq. (A2), we obtain

$$\lambda_3 = \frac{3m_h^2}{v}\left(1 + \frac{8v^2}{3m_h^2}\sum_{n=3}^{\infty}\frac{n(n-1)(n-2)c_{2n}v^{2(n-2)}}{2^n\Lambda^{2(n-2)}}\right), \quad \text{(A8)}$$

where $|c_{2n}| < 1$. This can be written as

$$\lambda_3 = \frac{3m_h^2}{v}\left(1 + \frac{8\Lambda^2}{3m_h^2v^2}\sum_{n=3}^{\infty}n(n-1)(n-2)c_{2n}\left(\frac{v^2}{2\Lambda^2}\right)^n\right). \quad \text{(A9)}$$

From this we clearly see that the series converges, even if all c_{2n} are 1, for

$$\Lambda > \frac{v}{\sqrt{2}} \sim 174 \text{ GeV}. \quad \text{(A10)}$$

APPENDIX B: MAXIMAL NEGATIVE ENHANCEMENTS OF λ_3 FOR $(\phi^\dagger\phi)^4$ AND $(\phi^\dagger\phi)^5$

The value of the triple Higgs coupling λ_3 is associated with the third derivative of the potential at the minimum, which corresponds to the change in the potential curvature. At the minimum of the Higgs potential at the VEV, the curvature value is a measured positive constant. Therefore, a negative λ_3 implies even lower curvatures for the higher values of ϕ. In the extreme case, where the curvature turns negative, this generates a maximum. Hence there has to be one more minimum for even higher values of ϕ so that the potential is stable in the limit of $\phi \to \infty$. Let the position of such a minimum be $\phi = p$.

This potential can be written as

$$v(\phi) = \frac{k_8}{8}(\phi^2 - v^2)^2(\phi^2 - p^2)^2 - \frac{k_8}{8}v^4p^4. \quad \text{(B1)}$$

Comparing this expression with the generic form of the Higgs potential, Eq. (16), we get

$$\frac{k_6}{6} = -\frac{3k_8}{4}(p^2 + v^2),$$
$$\frac{\lambda}{4} = -\frac{k_8}{8}(p^4 + v^4 + 4p^2v^2). \quad \text{(B2)}$$

Substituting this in Eq. (A5) we obtain a relation between k_8 and the Higgs mass, namely

$$k_8 = \frac{m_h^2}{v^2(p^2 - v^2)^2}. \quad \text{(B3)}$$

Substituting in Eq. (B2) gives

$$k_6 = -\frac{3m_h^2}{2v^2}\frac{(p^2 + v^2)}{(p^2 - v^2)^2}; \quad \text{(B4)}$$

k_8 has to be positive for the stability of the potential. Therefore k_6 is the only term that contributes to the enhancement with opposite sign. The maximal negative value it can take is, for $c_6 < 1$,

$$k_6 = -\frac{3}{4\Lambda^2}. \quad \text{(B5)}$$

Equating the right-hand sides of Eq. (B4) and Eq. (B5) yields

$$2m_h^2(p^2 + v^2)\Lambda^2 = (p^2 - v^2)^2v^2. \quad \text{(B6)}$$

Solving for p^2 gives

$$p^2 - v^2 = \frac{m_h^2\Lambda^2 \pm \sqrt{m_h^4\Lambda^4 + 4m_h^2\Lambda^2v^4}}{v^2}. \quad \text{(B7)}$$

The right-hand side must be greater than 0 as $p > v$. This implies

$$p^2 - v^2 = \frac{m_h\Lambda}{v^2}\left(m_h\Lambda + \sqrt{m_h^2\Lambda^2 + 4v^4}\right). \quad \text{(B8)}$$

From Eq. (A7), we know

$$\frac{\lambda_3}{\lambda_3^{\text{SM}}} - 1 = \frac{8v^4}{3m_h^2}(k_6 + 3k_8v^2). \quad \text{(B9)}$$

Substituting Eq. (B4) in Eq. (B9) gives

$$\frac{\lambda_3}{\lambda_3^{\rm SM}} - 1 = -\frac{4v^2}{p^2 - v^2}. \tag{B10}$$

$$\delta = \frac{\lambda_3}{\lambda_3^{\rm SM}} - 1 = -\frac{x}{1+\sqrt{1+x}}, \quad \text{where } x = \frac{4v^4}{m_h^2 \Lambda^2}. \tag{B11}$$

Using Eq. (B8), we get the maximum negative enhancement, namely

[1] G. Aad *et al.* (ATLAS Collaboration), Observation of a new particle in the search for the standard model Higgs boson with the ATLAS detector at the LHC, Phys. Lett. B **716**, 1 (2012).

[2] S. Chatrchyan *et al.* (CMS Collaboration), Observation of a new boson at a mass of 125 GeV with the CMS experiment at the LHC, Phys. Lett. B **716**, 30 (2012).

[3] G. Aad *et al.* (ATLAS and CMS Collaborations), Combined Measurement of the Higgs Boson Mass in pp Collisions at $\sqrt{s} = 7$ and 8 TeV with the ATLAS and CMS Experiments, Phys. Rev. Lett. **114**, 191803 (2015).

[4] CERN, Measurements of the Higgs boson production and decay rates and coupling strengths using pp collision data at $\sqrt{s} = 7$ and 8 TeV in the ATLAS experiment, Report No. ATLAS-CONF-2015-007, 2015.

[5] V. Khachatryan *et al.* (CMS Collaboration), Precise determination of the mass of the Higgs boson and tests of compatibility of its couplings with the standard model predictions using proton collisions at 7 and 8 TeV, Eur. Phys. J. C **75**, 212 (2015).

[6] A. Menon, D. E. Morrissey, and C. E. M. Wagner, Electroweak baryogenesis and dark matter in the nMSSM, Phys. Rev. D **70**, 035005 (2004).

[7] C. Grojean, G. Servant, and J. D. Wells, First-order electroweak phase transition in the standard model with a low cutoff, Phys. Rev. D **71**, 036001 (2005).

[8] A. Noble and M. Perelstein, Higgs self-coupling as a probe of electroweak phase transition, Phys. Rev. D **78**, 063518 (2008).

[9] V. Barger, D. J. H. Chung, A. J. Long, and L.-T. Wang, Strongly first order phase transitions near an enhanced discrete symmetry point, Phys. Lett. B **710**, 1 (2012).

[10] D. J. H. Chung, A. J. Long, and L.-T. Wang, 125 GeV Higgs boson and electroweak phase transition model classes, Phys. Rev. D **87**, 023509 (2013).

[11] A. Katz and M. Perelstein, Higgs couplings and electroweak phase transition, J. High Energy Phys. 07 (2014) 108.

[12] D. Curtin, P. Meade, and C.-T. Yu, Testing electroweak baryogenesis with future colliders, J. High Energy Phys. 11 (2014) 127.

[13] H.-J. He, J. Ren, and W. Yao, Probing new physics of cubic Higgs interaction via Higgs pair production at hadron colliders, Phys. Rev. D **93**, 015003 (2016).

[14] A. D. Sakharov, Violation of CP Invariance, c asymmetry, and baryon asymmetry of the Universe, Pis'ma Zh. Eksp. Teor. Fiz. **5**, 32 (1967) [JETP Lett. **5**, 24 (1967)]; A. D. Sakharov, Usp. Fiz. Nauk. **161**, 61 (1991) [Adv. Phys. Sci. (1991)].

[15] F. R. Klinkhamer and N. S. Manton, A saddle point solution in the Weinberg-Salam theory, Phys. Rev. D **30**, 2212 (1984).

[16] M. E. Shaposhnikov, Baryon asymmetry of the Universe in standard electroweak theory, Nucl. Phys. **B287**, 757 (1987).

[17] M. Dine, R. G. Leigh, P. Huet, A. D. Linde, and D. A. Linde, Comments on the electroweak phase transition, Phys. Lett. B **283**, 319 (1992).

[18] K. Kajantie, M. Laine, K. Rummukainen, and M. E. Shaposhnikov, The electroweak phase transition: a nonperturbative analysis, Nucl. Phys. **B466**, 189 (1996).

[19] R. Apreda, M. Maggiore, A. Nicolis, and A. Riotto, Gravitational waves from electroweak phase transitions, Nucl. Phys. **B631**, 342 (2002).

[20] C. Grojean and G. Servant, Gravitational waves from phase transitions at the electroweak scale and beyond, Phys. Rev. D **75**, 043507 (2007).

[21] J. R. Espinosa, T. Konstandin, J. M. No, and M. Quiros, Some cosmological implications of hidden sectors, Phys. Rev. D **78**, 123528 (2008).

[22] P. Binetruy, A. Bohe, C. Caprini, and J.-F. Dufaux, Cosmological backgrounds of gravitational eaves and eLISA/NGO: phase transitions, cosmic strings and other sources, J. Cosmol. Astropart. Phys. 06 (2012) 027.

[23] L. Leitao, A. Megevand, and A. D. Sanchez, Gravitational waves from the electroweak phase transition, J. Cosmol. Astropart. Phys. 10 (2012) 024.

[24] Y. Kikuta, K. Kohri, and E. So, Detecting the relic gravitational wave from the electroweak phase transition at SKA, arXiv:1405.4166.

[25] M. Kakizaki, S. Kanemura, and T. Matsui, Gravitational waves as a probe of extended scalar sectors with the first order electroweak phase transition, Phys. Rev. D **92**, 115007 (2015).

[26] R. Frederix, S. Frixione, V. Hirschi, F. Maltoni, O. Mattelaer, P. Torrielli, E. Vryonidou, and M. Zaro, Higgs pair production at the LHC with NLO and parton-shower effects, Phys. Lett. B **732**, 142 (2014).

[27] U. Baur, T. Plehn, and D. L. Rainwater, Probing the Higgs self coupling at hadron colliders using rare decays, Phys. Rev. D **69**, 053004 (2004).

[28] M. J. Dolan, C. Englert, and M. Spannowsky, Higgs self-coupling measurements at the LHC, J. High Energy Phys. 10 (2012) 112.

[29] J. Baglio, A. Djouadi, R. Grber, M. M. Mhlleitner, J. Quevillon, and M. Spira, The measurement of the Higgs

self-coupling at the LHC: theoretical status, J. High Energy Phys. 04 (2013) 151.
[30] M. J. Dolan, C. Englert, and M. Spannowsky, New physics in LHC Higgs boson pair production, Phys. Rev. D **87**, 055002 (2013).
[31] V. Barger, L. L. Everett, C. Jackson, and G. Shaughnessy, Higgs-pair production and measurement of the triscalar coupling at LHC(8,14), Phys. Lett. B **728**, 433 (2014).
[32] A. J. Barr, M. J. Dolan, C. Englert, and M. Spannowsky, Di-Higgs final states augMT2ed—selecting hh events at the high luminosity LHC, Phys. Lett. B **728**, 308 (2014).
[33] W. Yao, Studies of measuring Higgs self coupling with $HH \to b\bar{b}\gamma\gamma$ at the future hadron colliders, arXiv: 1308.6302.
[34] CERN, Prospects for measuring Higgs pair production in the channel $H(\to \gamma\gamma)H(\to b\bar{b})$ using the ATLAS detector at the HL-LHC, Report No. ATL-PHYS-PUB-2014-019, 2014.
[35] C.-T. Lu, J. Chang, K. Cheung, and J. S. Lee, A model independent analysis of Higgs-boson pair production at the LHC, J. High Energy Phys. 08 (2015) 133.
[36] A. G. Cohen, D. B. Kaplan, and A. E. Nelson, Progress in electroweak baryogenesis, Annu. Rev. Nucl. Part. Sci. **43**, 27 (1993).
[37] A. Riotto and M. Trodden, Recent progress in baryogenesis, Annu. Rev. Nucl. Part. Sci. **49**, 35 (1999).
[38] D. E. Morrissey and M. J. Ramsey-Musolf, Electroweak baryogenesis, New J. Phys. **14**, 125003 (2012).
[39] J. M. Cline, K. Kainulainen, and A. P. Vischer, Dynamics of two Higgs doublet CP violation and baryogenesis at the electroweak phase transition, Phys. Rev. D **54**, 2451 (1996).
[40] M. Carena, M. Quiros, and C. E. M. Wagner, Opening the window for electroweak baryogenesis, Phys. Lett. B **380**, 81 (1996).
[41] B. de Carlos and J. R. Espinosa, The baryogenesis window in the MSSM, Nucl. Phys. **B503**, 24 (1997).
[42] M. Carena, M. Quiros, and C. E. M. Wagner, Electroweak baryogenesis and Higgs and stop searches at LEP and the Tevatron, Nucl. Phys. **B524**, 3 (1998).
[43] M. Laine and K. Rummukainen, The MSSM electroweak phase transition on the lattice, Nucl. Phys. **B535**, 423 (1998).
[44] C. Delaunay, C. Grojean, and J. D. Wells, Dynamics of nonrenormalizable electroweak symmetry breaking, J. High Energy Phys. 04 (2008) 029.
[45] M. Carena, G. Nardini, M. Quiros, and C. E. M. Wagner, The baryogenesis window in the MSSM, Nucl. Phys. **B812**, 243 (2009).
[46] T. Cohen and A. Pierce, Electroweak baryogenesis and colored scalars, Phys. Rev. D **85**, 033006 (2012).
[47] M. Laine, G. Nardini, and K. Rummukainen, Lattice study of an electroweak phase transition at m · h 126 GeV, J. Cosmol. Astropart. Phys. 01 (2013) 011.
[48] D. Curtin, P. Jaiswal, and P. Meade, Excluding electroweak baryogenesis in the MSSM, J. High Energy Phys. 08 (2012) 005.
[49] M. Carena, G. Nardini, M. Quiros, and C. E. M. Wagner, MSSM electroweak baryogenesis and LHC data, J. High Energy Phys. 02 (2013) 001.
[50] M. Carena, A. Megevand, M. Quiros, and C. E. M. Wagner, Electroweak baryogenesis and new TeV fermions, Nucl. Phys. **B716**, 319 (2005).
[51] W. Huang, J. Shu, and Y. Zhang, On the Higgs fit and electroweak phase transition, J. High Energy Phys. 03 (2013) 164.
[52] R. Fok and G. D. Kribs, Four generations, the electroweak phase transition, and supersymmetry, Phys. Rev. D **78**, 075023 (2008).
[53] H. Davoudiasl, I. Lewis, and E. Ponton, Electroweak phase transition, Higgs diphoton rate, and new heavy fermions, Phys. Rev. D **87**, 093001 (2013).
[54] M. Gorbahn, J. M. No, and V. Sanz, Benchmarks for Higgs effective theory: Extended Higgs sectors, J. High Energy Phys. 10 (2015) 036.
[55] M. Pietroni, The electroweak phase transition in a non-minimal supersymmetric model, Nucl. Phys. **B402**, 27 (1993).
[56] A. T. Davies, C. D. Froggatt, and R. G. Moorhouse, Electroweak baryogenesis in the next-to-minimal supersymmetric model, Phys. Lett. B **372**, 88 (1996).
[57] S. J. Huber, T. Konstandin, T. Prokopec, and M. G. Schmidt, Electroweak phase transition and baryogenesis in the nMSSM, Nucl. Phys. **B757**, 172 (2006).
[58] M. Carena, N. R. Shah, and C. E. M. Wagner, Light dark matter and the electroweak phase transition in the NMSSM, Phys. Rev. D **85**, 036003 (2012).
[59] W. Huang, Z. Kang, J. Shu, P. Wu, and J. M. Yang, New insights in the electroweak phase transition in the NMSSM, Phys. Rev. D **91**, 025006 (2015).
[60] T. Corbett, O. J. P. Eboli, J. Gonzalez-Fraile, and M. C. Gonzalez-Garcia, Robust determination of the Higgs couplings: power to the data, Phys. Rev. D **87**, 015022 (2013).
[61] F. Goertz, A. Papaefstathiou, L. L. Yang, and J. Zurita, Higgs boson pair production in the $D = 6$ extension of the SM, J. High Energy Phys. 04 (2015) 167.
[62] A. Azatov, R. Contino, G. Panico, and M. Son, Effective field theory analysis of double Higgs boson production via gluon fusion, Phys. Rev. D **92**, 035001 (2015).
[63] X.-m. Zhang, Operators analysis for Higgs potential and cosmological bound on Higgs mass, Phys. Rev. D **47**, 3065 (1993).
[64] F. P. Huang, P.-H. Gu, P.-F. Yin, Z.-H. Yu, and X. Zhang, Testing the electroweak phase transition and electroweak baryogenesis at LHC and CEPC, arXiv:1511.03969.
[65] R. S. Gupta, H. Rzehak, and J. D. Wells, How well do we need to measure the Higgs boson mass and self coupling?, Phys. Rev. D **88**, 055024 (2013).
[66] S. Profumo, M. J. Ramsey-Musolf, and G. Shaughnessy, Singlet Higgs phenomenology and the electroweak phase transition, J. High Energy Phys. 08 (2007) 010.
[67] V. Barger, P. Langacker, M. McCaskey, M. J. Ramsey-Musolf, and G. Shaughnessy, LHC phenomenology of an extended standard model with a real scalar singlet, Phys. Rev. D **77**, 035005 (2008).
[68] C. L. Wainwright, S. Profumo, and M. J. Ramsey-Musolf, Phase transitions and gauge artifacts in an Abelian Higgs plus singlet model, Phys. Rev. D **86**, 083537 (2012).

[69] H. H. Patel and M. J. Ramsey-Musolf, Stepping into electroweak symmetry breaking: phase transitions and Higgs phenomenology, Phys. Rev. D **88**, 035013 (2013).
[70] J. M. No and M. Ramsey-Musolf, Probing the Higgs portal at the LHC through resonant di-Higgs production, Phys. Rev. D **89**, 095031 (2014).
[71] S. Profumo, M. J. Ramsey-Musolf, C. L. Wainwright, and P. Winslow, Singlet-catalyzed electroweak phase transitions and precision Higgs boson studies, Phys. Rev. D **91**, 035018 (2015).
[72] J. Kozaczuk, Bubble expansion and the viability of singlet-driven electroweak baryogenesis, J. High Energy Phys. 10 (2015) 135.
[73] J. Kozaczuk, S. Profumo, L. S. Haskins, and C. L. Wainwright, Cosmological phase transitions and their properties in the NMSSM, J. High Energy Phys. 01 (2015) 144.
[74] D. Buttazzo, F. Sala, and A. Tesi, Singlet-like Higgs bosons at present and future colliders, J. High Energy Phys. 11 (2015) 158.
[75] The ATLAS and CMS Collaboration, Report No. ATLAS-CONF-2015-007.
[76] V. Khachatryan *et al.* (CMS Collaboration), Search for a Higgs Boson in the Mass Range from 145 to 1000 GeV Decaying to a Pair of W or Z Bosons, J. High Energy Phys. 10 (2015) 144.
[77] T. Robens and T. Stefaniak, Status of the Higgs singlet extension of the standard model after LHC run 1, Eur. Phys. J. C **75**, 104 (2015).
[78] D. Lopez-Val and T. Robens, Delta r and the W-boson mass in the singlet extension of the standard model, Phys. Rev. D **90**, 114018 (2014).
[79] CDF, D0 Collaboration, T. E. W. Group, 2012 update of the combination of CDF and D0 results for the mass of the W boson, arXiv:1204.0042.
[80] J. Alcaraz *et al.* (DELPHI, OPAL, ALEPH, LEP Electroweak Working Group, L3 Collaboration), A combination of preliminary electroweak measurements and constraints on the standard model, arXiv:hep-ex/0612034.
[81] T. Aaltonen *et al.* (CDF Collaboration), Precise Measurement of the W-Boson Mass with the CDF II Detector, Phys. Rev. Lett. **108**, 151803 (2012).
[82] V. M. Abazov *et al.* (D0 Collaboration), Measurement of the W Boson Mass with the D0 Detector, Phys. Rev. Lett. **108**, 151804 (2012).
[83] W. J. Marciano and A. Sirlin, Radiative corrections to neutrino-induced neutral-current phenomena in the $\mathrm{SU}(2)_L \times \mathrm{U}(1)$ theory, Phys. Rev. D **22**, 2695 (1980).
[84] M. Awramik, M. Czakon, A. Freitas, and G. Weiglein, Precise prediction for the W boson mass in the standard model, Phys. Rev. D **69**, 053006 (2004).
[85] G. Degrassi, P. Gambino, and P. P. Giardino, The $m_W - m_Z$ interdependence in the standard model: a new scrutiny, J. High Energy Phys. 05 (2015) 154.
[86] K. Hagiwara, S. Matsumoto, D. Haidt, and C. S. Kim, A novel approach to confront electroweak data and theory, Z. Phys. C **64**, 559 (1994); **68**, 352 (1995).
[87] C.-Y. Chen, S. Dawson, and I. M. Lewis, Exploring resonant di-Higgs boson production in the Higgs singlet model, Phys. Rev. D **91**, 035015 (2015).
[88] S. Dittmaier *et al.* (LHC Higgs Cross Section Working Group Collaboration), Handbook of LHC Higgs cross sections: 1. Inclusive observables, arXiv:1101.0593.
[89] G. F. Giudice, C. Grojean, A. Pomarol, and R. Rattazzi, The strongly interacting light Higgs, J. High Energy Phys. 06 (2007) 045.
[90] E. N. Glover and J. van der Bij, Higgs boson pair production via gluon fusion, Nucl. Phys. **B309**, 282 (1988).
[91] D. A. Dicus, C. Kao, and S. S. Willenbrock, Higgs boson pair production from gluon fusion, Phys. Lett. B **203**, 457 (1988).
[92] T. Plehn, M. Spira, and P. Zerwas, Pair production of neutral Higgs particles in gluon-gluon collisions, Nucl. Phys. **B479**, 46 (1996).
[93] S. Dawson, S. Dittmaier, and M. Spira, Neutral Higgs boson pair production at hadron colliders: QCD corrections, Phys. Rev. D **58**, 115012 (1998).
[94] B. A. Kniehl and M. Spira, Low-energy theorems in Higgs physics, Z. Phys. C **69**, 77 (1995).
[95] D. de Florian and J. Mazzitelli, Two-loop virtual corrections to Higgs pair production, Phys. Lett. B **724**, 306 (2013).
[96] D. de Florian and J. Mazzitelli, Higgs Boson Pair Production at Next-to-Next-to-Leading Order in QCD, Phys. Rev. Lett. **111**, 201801 (2013).
[97] J. Grigo, K. Melnikov, and M. Steinhauser, Virtual corrections to Higgs boson pair production in the large top quark mass limit, Nucl. Phys. **B888**, 17 (2014).
[98] D. de Florian and J. Mazzitelli, Higgs pair production at next-to-next-to-leading logarithmic accuracy at the LHC, J. High Energy Phys. 09 (2015) 053.
[99] D. Y. Shao, C. S. Li, H. T. Li, and J. Wang, Threshold resummation effects in Higgs boson pair production at the LHC, J. High Energy Phys. 07 (2013) 169.
[100] S. Dawson, A. Ismail, and I. Low, What's in the loop? The anatomy of double Higgs production, Phys. Rev. D **91**, 115008 (2015).
[101] B. Batell, M. McCullough, D. Stolarski, and C. B. Verhaaren, Putting a stop to di-Higgs modifications, J. High Energy Phys. 09 (2015) 216.
[102] J. M. Campbell and R. Ellis, MCFM for the Tevatron and the LHC, Nucl. Phys. B, Proc. Suppl. **205–206**, 10 (2010).
[103] T. Sjostrand, S. Mrenna, and P. Z. Skands, A brief introduction to PYTHIA 8.1, Comput. Phys. Commun. **178**, 852 (2008).
[104] J. de Favereau, C. Delaere, P. Demin, A. Giammanco, V. Lemaître, A. Mertens, and M. Selvaggi (DELPHES 3 Collaboration), DELPHES 3, a modular framework for fast simulation of a generic collider experiment, J. High Energy Phys. 02 (2014) 057.
[105] J. Alwall, R. Frederix, S. Frixione, V. Hirschi, F. Maltoni, O. Mattelaer, H.-S. Shao, T. Stelzer, P. Torrielli, and M. Zaro, The automated computation of tree-level and next-to-leading order differential cross sections, and their matching to parton shower simulations, J. High Energy Phys. 07 (2014) 079.
[106] CMS Collaboration, Projected performance of an upgraded CMS detector at the LHC and HL-LHC: contribution to the Snowmass process, arXiv:1307.7135.

[107] G. Aad *et al.* (ATLAS Collaboration), Expected performance of the ATLAS experiment—detector, trigger and physics, arXiv:0901.0512.

[108] CMS Collaboration, Higgs pair production at the High Luminosity LHC, Report No. CMS-PAS-FTR-15-002.

[109] A. J. Barr, M. J. Dolan, C. Englert, D. E. Ferreira de Lima, and M. Spannowsky, Higgs self-coupling measurements at a 100 TeV hadron collider, J. High Energy Phys. 02 (2015) 016.

[110] A. Elagin, P. Murat, A. Pranko, and A. Safonov, A new mass reconstruction technique for resonances decaying to di-tau, Nucl. Instrum. Methods Phys. Res., Sect. A **654**, 481 (2011).

[111] S. Chatrchyan *et al.* (CMS Collaboration), Observation of a new boson at a mass of 125 GeV with the CMS experiment at the LHC, Phys. Lett. B **716**, 30 (2012).

[112] G. Aad *et al.* (ATLAS Collaboration), Observation of a new particle in the search for the standard model Higgs boson with the ATLAS detector at the LHC, Phys. Lett. B **716**, 1 (2012).